23. Monotectic and Syntectic Alloys

Experiment MA-044

L. L. Lacy [a] *and C. Y. Ang*[ab]

ABSTRACT

The flight test furnace run of the Monotectic and Syntectic Alloys Experiment was successfully conducted during the Apollo-Soyuz Test Project mission in July 1975. Examination of the returned sample cartridges and the formal comparative characterization of the low-g- and one-g-processed samples of lead-zinc and aluminum antimonide have been completed. The results on aluminum antimonide show that polycrystalline and multiphased material can be homogenized in space under low-g conditions. In terms of reduction of the unwanted second phase, the low-g samples show a homogeneity improvement by factors from 4 to 20 over the one-g counterparts. Furthermore, small amounts of the second phase were formed only along parts of the grain boundaries of the flight samples, whereas the ground-based samples show major grains of the second phase.

Microstructural study on the lead-zinc flight samples shows that complete interdiffusion of lead and zinc had not been achieved, even though the flight data indicated a soak temperature in the miscible region that was 40 K above the published consolute temperature. Dispersion of lead particles in the zinc matrix was observed in both the low-g and one-g samples of lead-zinc. A chemical analysis of cut sections shows that the distribution of lead in zinc in the flight sample follows a diffusional process with a diffusion coefficient of $\approx 3 \times 10^{-6}$ cm^2/sec, which is about two orders of magnitude smaller than that for miscible liquid metals. Conversely, the one-g samples of lead-zinc have a uniform, dilute concentration of lead in the zinc matrix, an indication that most of the lead phase was removed by sedimentation after it was introduced by convective mixing.

INTRODUCTION

Certain potentially useful alloys or material systems are difficult to synthesize on Earth because of sizable differences in specific gravity of the constituents in a molten state; these differences result in undesirable buoyancy and convection influences during homogenization of the melts as well as during the initial stages of solidification and grain growth. Consequently, the near-zero-g condition in space processing was the primary motivation for this experiment. Furthermore, significant discoveries related to microsegregation and kinetics of lattice defects, made as a result of Skylab experiments (refs. 23-1 and 23-2), have shown the value of continuing space-processing experimentation for future manufacturing activities in space.

The purpose of this experiment was to investigate the effects of weightlessness on the melting and solidification of two material systems, lead-zinc (Pb-Zn) and aluminum antimonide (AlSb). The objectives were (1) to investigate phase segregation effects in low g for the immiscible binary Pb-Zn and (2) to determine the influences of low-g solidification on the microstructural homogeneity and stoichiometry of the semiconducting compound AlSb. This report contains a

[a]NASA George C. Marshall Space Flight Center; Co-Principal Investigators.

[b]Universities Space Research Association, visiting scientist at George C. Marshall Space Flight Center.

comprehensive summary of evaluation results for two flight samples, two ground-based tested (GBT) samples, and two prototype tested (PT) samples of each material. Additional samples were used for specific tests such as chemical analyses.

EXPERIMENT CONCEPT AND PROCEDURES

The Pb-Zn monotectic system (ref. 23-3 and fig. 23-1) is characterized by the large miscibility gap $L_1 + L_2$ in which liquid phases can coexist over a large compositional and temperature range. This system is also characterized by a large density difference between Pb (11.7 g/cm^3) and Zn (7.14 g/cm^3). In the Earth's gravity field, the prevention of gravity separation between Pb and Zn upon solidification is difficult. Negating the effects of gravity in space processing should lead to an optimum mixing of the two phases, resulting in a dispersion of fine particles of superconducting Pb in a Zn-rich composition. Previous results of Apollo 14 (ref. 23-4), Skylab (refs. 23-1, 23-2, and 23-5), and experiments performed on the NASA George C. Marshall Space Flight Center (MSFC) drop tower (refs. 23-6 to 23-8) indicated that stable dispersions of immiscible liquids can be prepared in a low-g environment, whereas similar dispersions prepared on Earth are rapidly separated by such gravity-dependent influences as creaming,

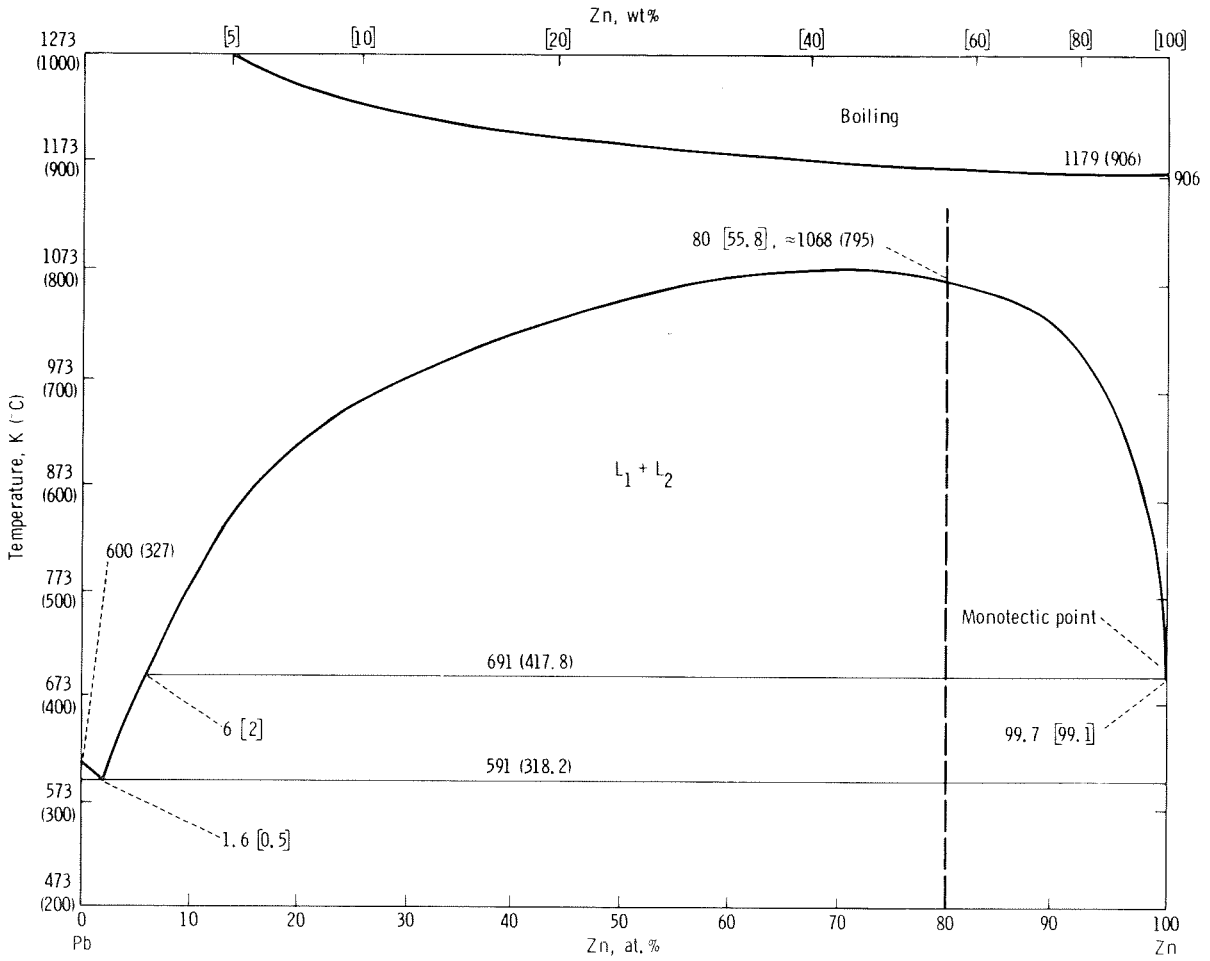

FIGURE 23-1.—Phase diagram for Pb-Zn.

flocculation, and coalescence. The composition selected for the experiment was 20 atomic percent (at.%) Pb and 80 at.% Zn, as shown by the heavy vertical line in figure 23-1. This composition is equivalent to a weight percent (wt%) of 44.2 Pb and 55.8 Zn or a volume percent of 33.2 Pb and 66.8 Zn.

The Pb-Zn samples were prepared from 99.999-percent-pure materials, which were premelted by heating (at a temperature of 1123 K (850° C)) the samples above the consolute temperature of the binary (1068 K (795° C)) for 10 minutes. Metallographic examination of the PT and GBT samples indicated good interfacial bonds between the gravity-separated layers. To obtain the low-g dispersions of Pb in Zn, the material was again heated 40 K (40° C) above the published value of the consolute temperature and allowed to inter-diffuse for 1.5 hours. A thermal history of Pb-Zn for both GBT and flight samples is shown by the

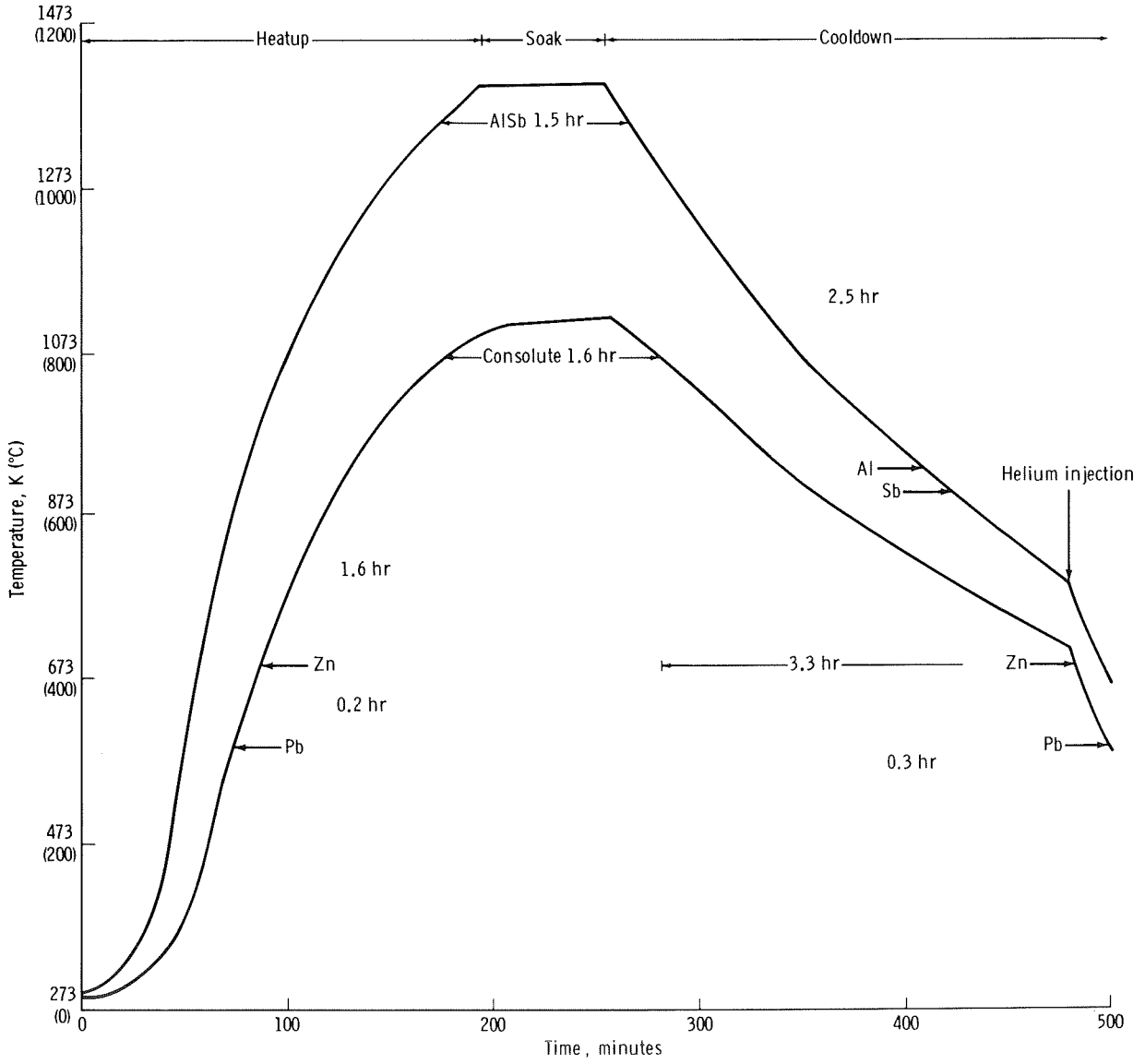

FIGURE 23-2.—Thermal history for AlSb and Pb-Zn.

lower curve in figure 23-2. Preflight diffusion analysis indicated that the liquid binary should be easily homogenized into single liquid phase within the 1.5-hour period. During the cooldown portion of the thermal history, it was anticipated that small Pb-rich liquid particles would continuously nucleate and grow in a Zn-rich liquid phase until the monotectic temperature was reached. Therefore, an objective of this investigation was to study the low-g diffusion and kinetics of such dispersions.

The AlSb system (fig. 23-3) has been neglected for many years among the Group III-V semiconducting compounds that are characterized upon solidification by a syntectic transformation of two molten constituents to a constant-composition intermetallic compound (50 at.% Al and 50 at.% Sb). The reasons for this neglect have been difficulties in synthesizing a stoichiometrically homogeneous compound and the problems of high reactivity of the material to moisture (ref. 23-9). With an energy gap of 1.62 eV, AlSb has been theoretically analyzed as a highly efficient solar cell material (refs. 23-10 and 23-11) that may be 30 to 50 percent more efficient than silicon.

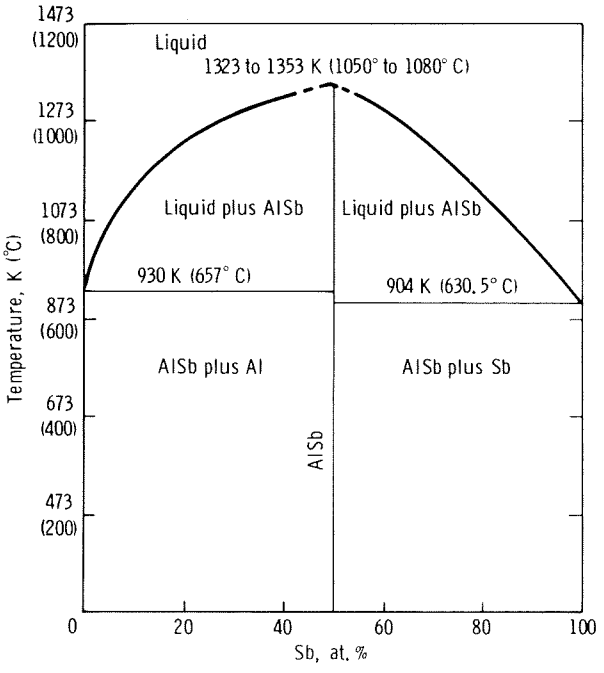

FIGURE 23-3.—Phase diagram for AlSb.

A typical grain of the best commercially available polycrystalline AlSb can be seen in figure 23-4. In addition to the compound phase, the material consists of Al- and Sb-rich phases. A chemical analysis of a 2-gram sample of this starting material indicated that macroscopically, the material has the correct stoichiometric composition of 50.00 at.% of each element and no more than 0.001 wt% oxygen content. In space processing, the compositional homogeneity may be enhanced by minimizing the very large density difference between constituents (2.7 g/cm^3 for Al and 6.62 g/cm^3 for Sb) in the molten state and during crystallite formation upon cooling. Electromotive potential considerations suggest that Al- and Sb-rich phases observed in polycrystalline AlSb synthesized on Earth could cause the high reactivity to moisture. Therefore, an objective of this

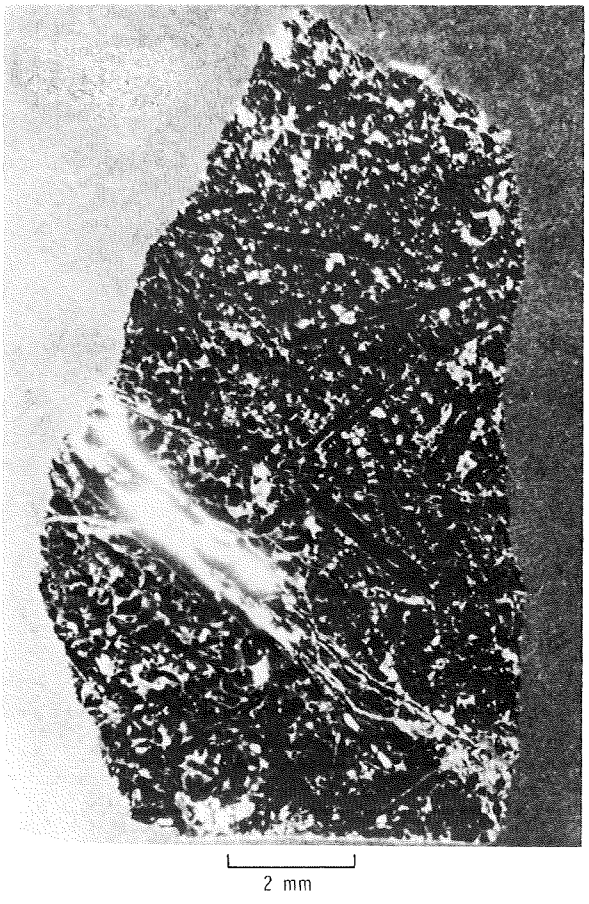

FIGURE 23-4.—Typical grain of AlSb starting material.

investigation was to determine whether low-g, liquid-state homogenization and solidification would improve the microstructural and compositional homogeneity of the best commercially available polycrystalline AlSb. A thermal history of the AlSb samples for both flight and GBT is given by the upper curve of figure 23-2. The experiment consisted of heating samples of polycrystalline AlSb 50 K (50° C) above the melting temperature (1353 K (1080° C)) for 1 hour.

A detailed description of sample preparation and experiment design for the ampoules and cartridges can be found in references 23-12 and 23-13. The AlSb and Pb-Zn samples were thermally cycled in the Apollo-Soyuz Test Project (ASTP) multipurpose furnace, which had three furnace cavities; each cavity provided a short hot zone and a longer gradient zone. As shown in figure 23-5, each furnace cartridge contained one AlSb and one Pb-Zn ampoule. Except for the difference in size, the two types of ampoules were similarly constructed. All sample preparation and ampoule assembly steps, from graphite crucible capping to tungsten-inert-gas welding of the stainless steel containers, were performed in an atmosphere of ultrapure argon gas. Similarly, assembled sample cartridges were thermally processed on the ground under one-g conditions for comparative characterization purposes. The post-ASTP and post-ground-test examination of cartridges and ampoules, including the quick-look evaluation of a limited number of samples, has been previously reported (refs. 23-12 and 23-13).

EXPERIMENTAL RESULTS AND DISCUSSION

Although the common denominator for both the AlSb and the Pb-Zn experiments is the study of effects of low g on liquid-state heat treatment and solidification, the two types of material

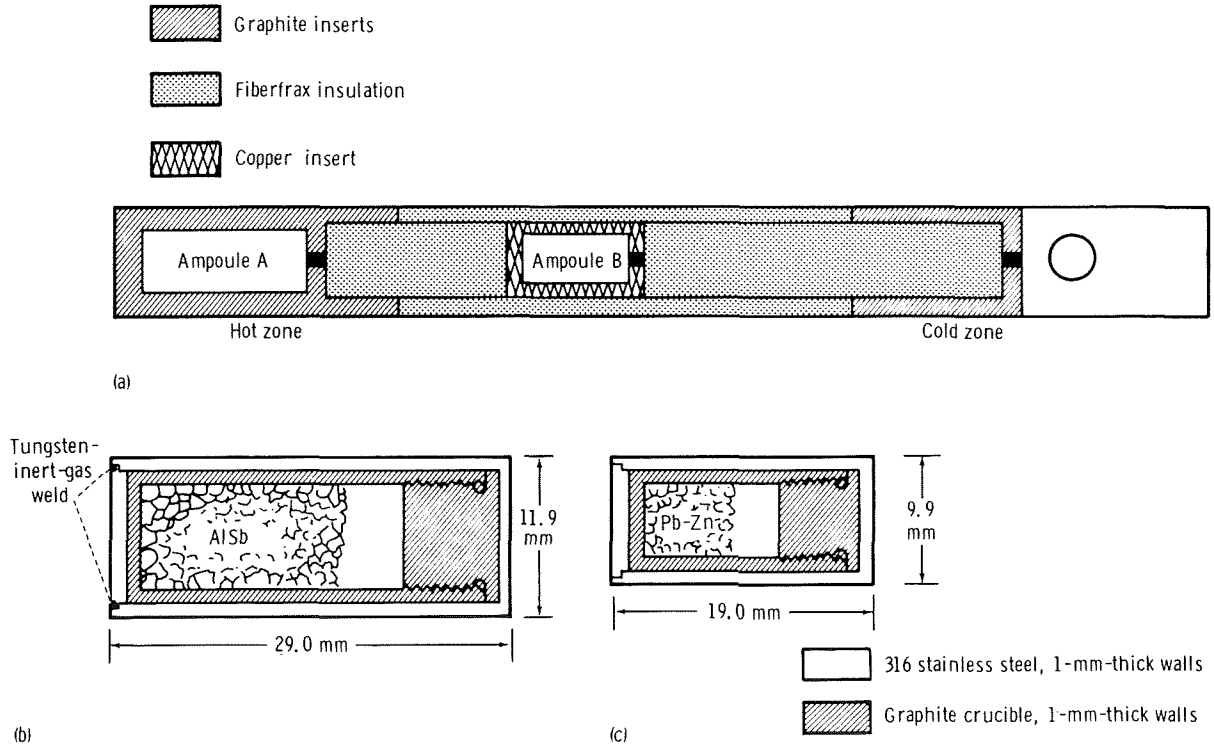

FIGURE 23-5.—Schematic of cartridge assembly and ampoules. (a) Stainless steel cartridge assembly. (b) Ampoule A (AlSb). (c) Ampoule B (Pb-Zn).

systems are quite different in terms of phase equilibria, phase transformations, and anticipated microstructure and properties. Therefore, the experimental results and analyses of the two materials are presented separately in the following discussion.

Thermal History

The soak temperatures of the flight and GBT samples were determined by using thermocouples attached directly to the experiment ampoules in instrumented prototype tests. Ampoule temperatures in the PT were determined as a function of two temperatures simultaneously measured inside the multipurpose furnace. The two temperatures measured in the furnace are at the hot end and the cold end of the experiment cartridges. Thus, the thermal history of the flight and GBT samples, shown in figure 23-2, was indirectly calculated from the measured furnace temperature data shown in figure 23-6. In figure 23-6, the hot- and cold-end furnace data for the flight

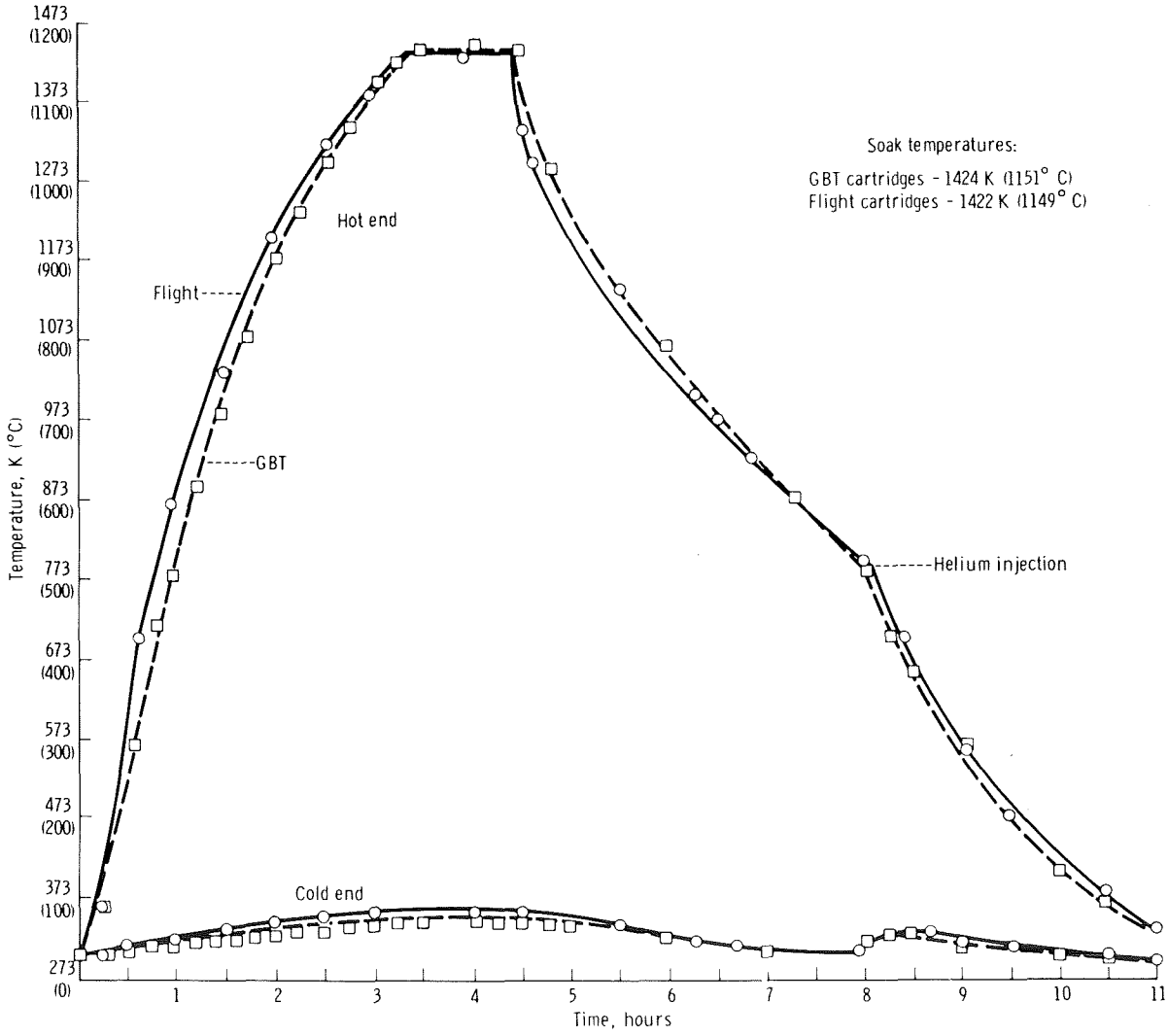

FIGURE 23-6.—Hot-end and cold-end temperatures of experiment cartridges.

and GBT cartridges are compared. The data of figure 23-6 indicate that the flight and GBT samples had essentially equivalent thermal histories.

Aluminum Antimonide Compound

The results of the AlSb experiment are discussed in the following paragraphs.

Postflight evaluation and characterization.—The postflight evaluation and characterization plan for the flight and GBT samples is given in table 23-I. A detailed discussion of task 1 and task 2 and a quick-look metallographic assessment of one flight sample (A-185) and one prototype sample (A-127) of AlSb are given in reference 23-12. A preliminary analysis of one flight sample (A-185), one GBT sample (A-141), and two PT samples of AlSb can be found in reference 23-13. The completed characterization of the previously mentioned samples and of additional flight, GBT, and PT samples is reviewed here. The characterization tasks to be discussed include metallography, quantitative microstructural analysis, scanning electron microscopy/energy dispersive X-ray analysis (SEM/EDAX), electrical resistivity

TABLE 23-I.—Postflight Evaluation and Characterization Plan

Evaluation	*AlSb*	*Pb-Zn*
Cartridge examination (task 1)		
Photography	X	X
Radiography (preflight and postflight)	X	X
Disassembly	X	X
Ampoule examination (task 2)		
Photography	X	X
Radiography	X	X
Leak tests (helium)	X	X
Weighing	X	X
Sample characterization (task 3)		
Removal	X	X
Weighing	X	X
Stereoscopic examination (10× to 100×)	X	X
Macrophotography (2× to 10×)	X	X
SEM[a] topography (60× to 1000×)		X
Surface EDAX[b]		X
Microstructure (metallography)	X	X
Quantitative microstructural analysis	X	X
SEM/EDAX (qualitative and quantitative)	X	X
Microhardness testing	X	
Resistivity (4-point probe)	X	X
X-ray diffraction	X	X
Chemical and spectral analysis	X	X
Microchemical analysis (ion microprobe)	X	X
Diffusion analysis	X	X

[a]Scanning electron microscope.
[b]Energy dispersive X-ray analysis.

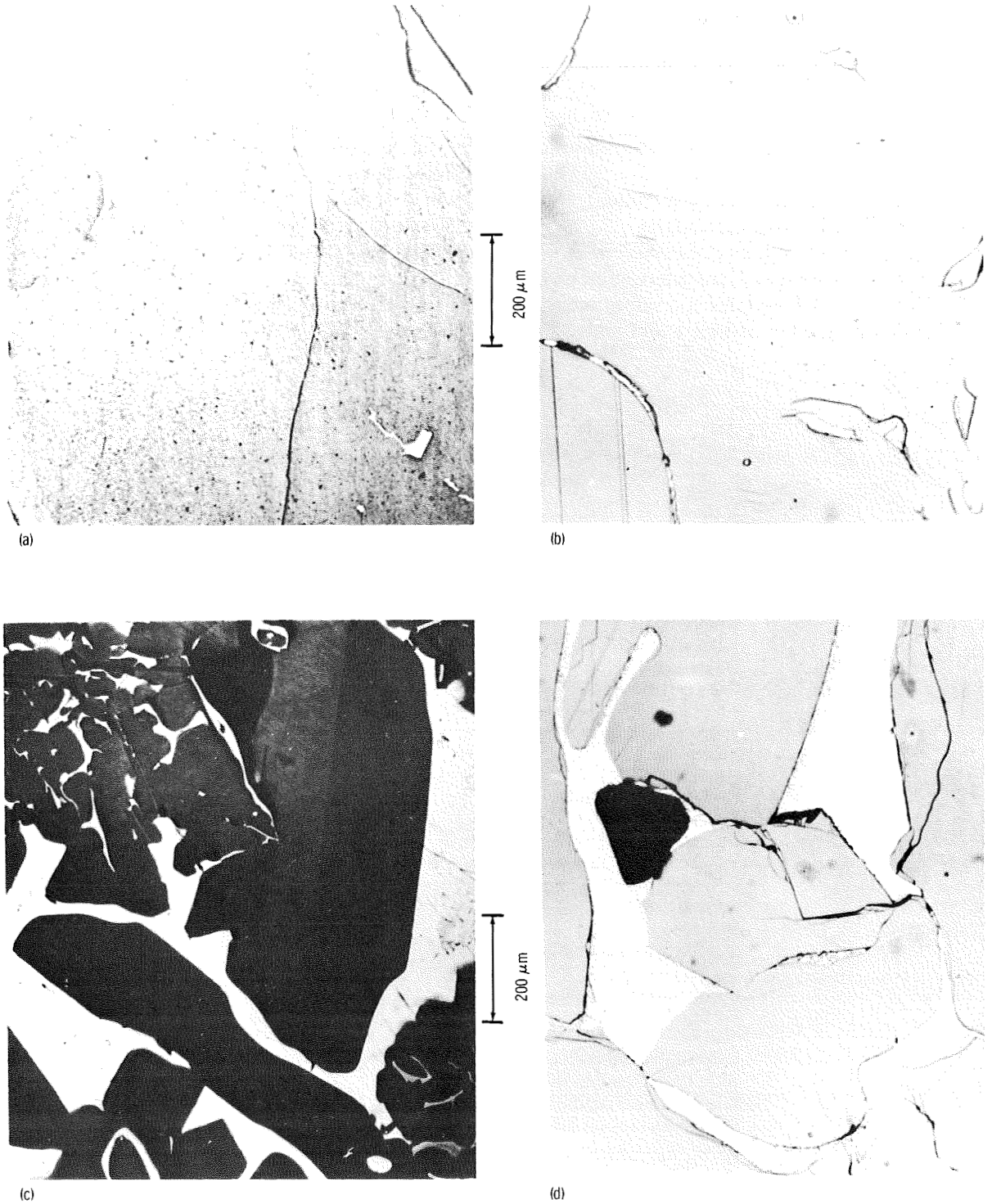

FIGURE 23-7.—Microstructures of low-g and one-g AlSb samples, showing difference in amounts of the primary grains (dark regions) and secondary phases. (a) Low-g sample (A-185). (b) Low-g sample (A-164). (c) One-g sample (PT). (d) One-g sample (GBT).

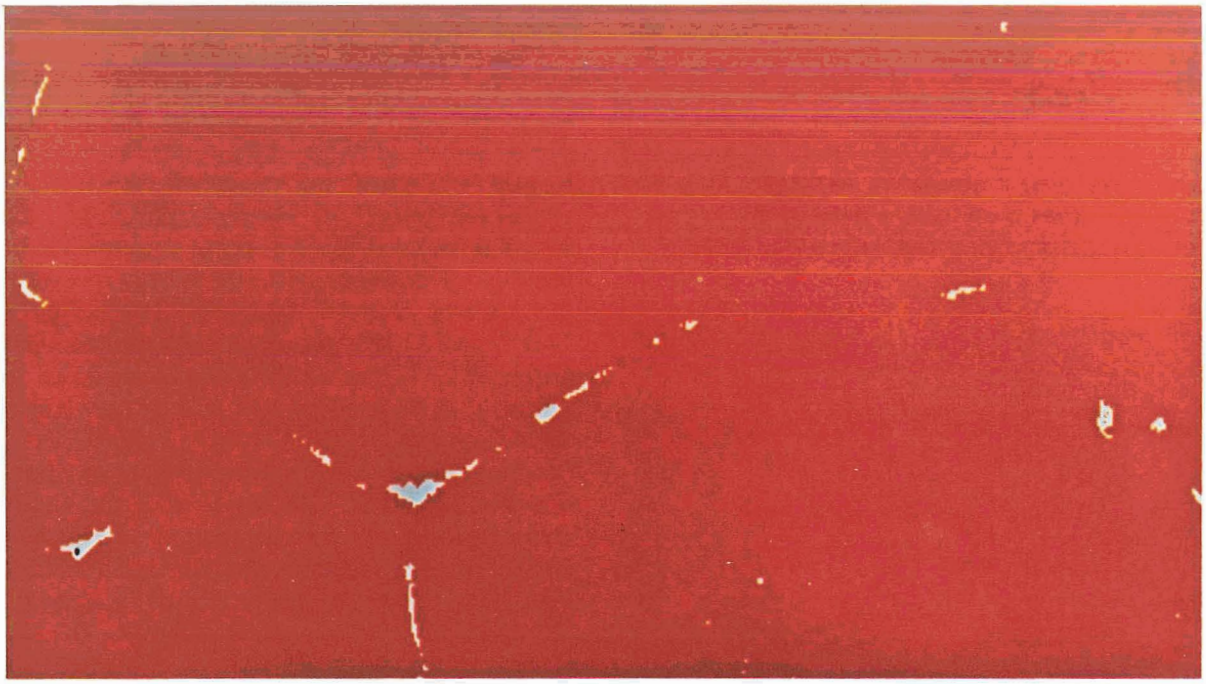

(a)

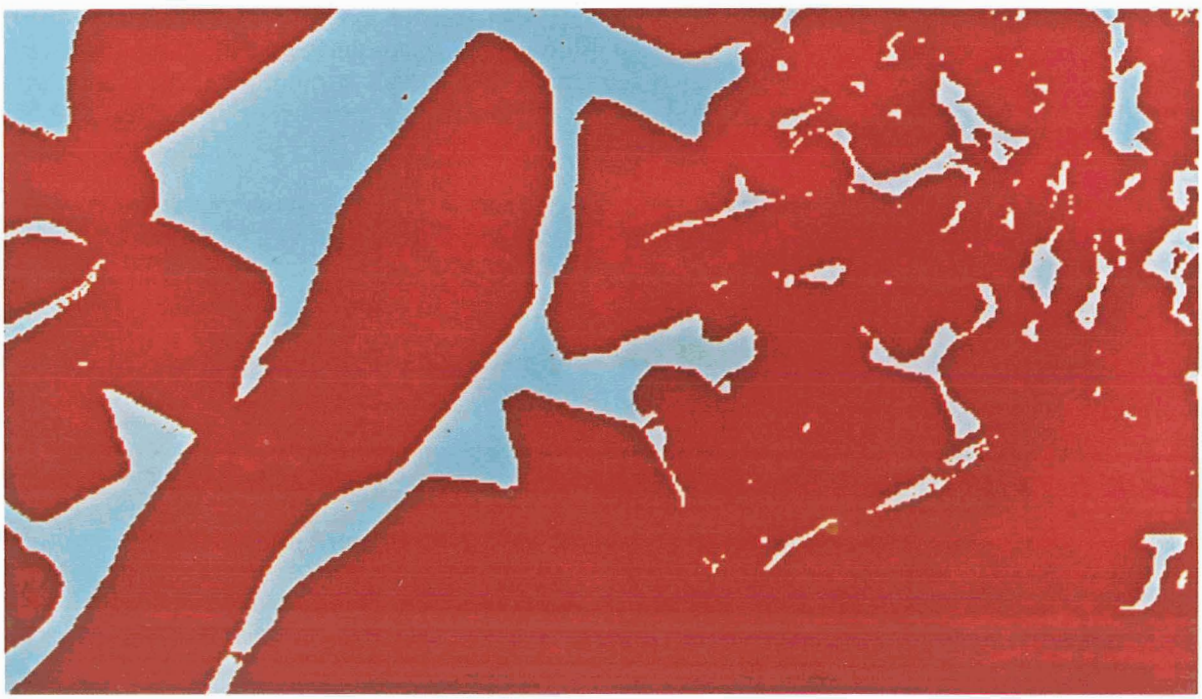

(b)

FIGURE 23-8.—Pseudocolor photographs showing microstructures of flight and PT AlSb samples. The red areas represent AlSb; the blue areas represent a second phase. (a) ASTP sample (A-185). Blue is Al-rich phase. (b) Laboratory sample (PT). Blue is Sb-rich phase.

measurements, X-ray diffraction studies, chemical analysis, and ion-microprobe mass analysis (IMMA).

Metallography and qualitative microanalysis.—A comparison of the microstructures of low-g and one-g samples is presented in figure 23-7. The typical unetched microstructure of low-g homogenized AlSb as represented by ASTP samples A-185 and A-164 in figures 23-7(a) and 23-7(b), respectively, shows that the very small amounts of a second phase (light) are formed along parts of the boundaries of the primary grains (dark) of AlSb compound. In contrast, figures 23-7(c) and 23-7(d), which represent the typical microstructures of the PT and GBT AlSb samples, respectively, show large amounts of the secondary phases not unlike the microstructure of the starting material. (See fig. 23-4.) Figures 23-8(a) and 23-8(b) are pseudocolor photographs of figures 23-7(a) and 23-7(c) in which surface artifacts have been eliminated and the computer-aided technique of digital imaging analysis (DIA) has been used to more clearly present compositional homogeneity. The red areas of the photograph represent the AlSb compound, and the blue areas represent a second phase (Al-rich for the flight sample and Sb-rich for the one-g sample). For these two selected photomicrographs, the area fraction of the secondary phase is 21.6 percent in the one-g sample and 1.7 percent in the flight sample.

Major improvements in microscopic homogeneity are quite evident in the flight samples. The EDAX maps of the one-g and low-g samples, shown respectively in figures 23-9 and

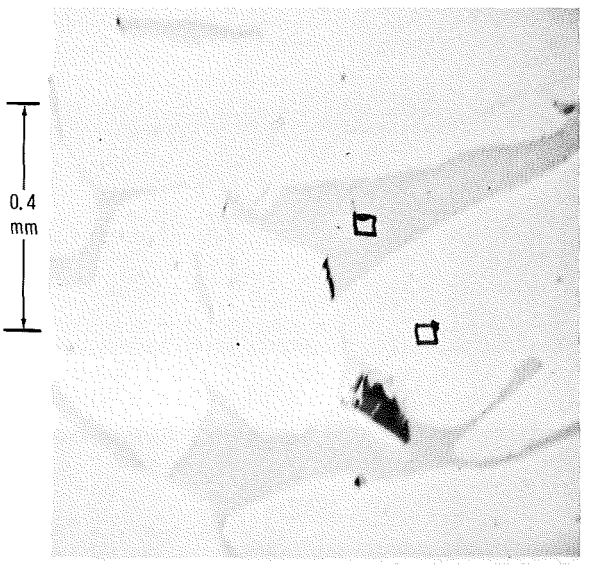

(a)

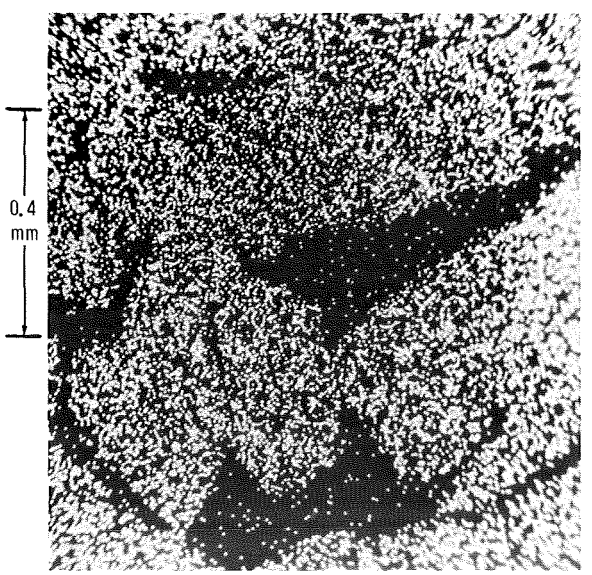

(b)

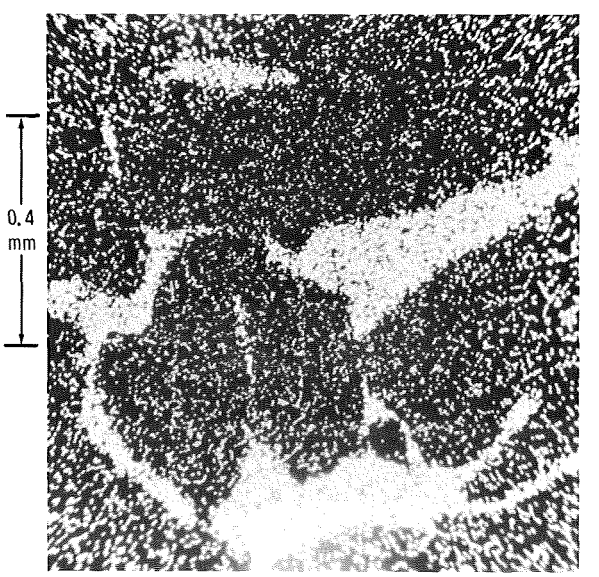

(c)

FIGURE 23-9.—SEM/EDAX map of GBT AlSb sample (A-141). (a) SEM photograph. (b) EDAX Sb scan. (c) EDAX Al scan.

23-10, qualitatively identify the gray phase as the compound AlSb and the white phase as an Al-rich phase. (In the SEM photographs (figs. 23-9(a) and 23-10(c)), the secondary phase appears lighter than the compound phase.) Figure 23-11 is a pseudocolor representation of the low-g and equivalent one-g microstructures using DIA. An analysis of the area fraction of the second phase for these two photomicrographs reveals that the flight sample has 1.1 percent of the Al-rich phase as compared to 25.2 percent for the GBT sample. Thus, for these two selected areas, the Al-rich phase has been reduced by a factor of 23 in the flight sample. Although the photomicrographs represent two selected locations of approximately 1 mm^2 surface area for the flight and GBT sample, the microstructures typify the salient features observed on a microscopic scale in other parts of the samples. That is, only a small amount of a secondary phase is found along parts of the AlSb grain boundaries for the flight sample, whereas major grains of a secondary or satellite phase are observed in the GBT sample.

To compare the homogeneity of the flight, GBT, and PT samples on a macroscopic scale, figure 23-12 is presented to show the relative location and size of the primary compound phase (red) and secondary phases (blue), determined using a 20-μm scan across the sample surfaces. The major improvement in macroscopic homogeneity of the flight sample is again evident. The size of the secondary phases for the PT and GBT samples can vary from less than 20 μm to as much as 1 mm, whereas the size of the secondary phase can vary from 3 to approximately 30 μm in the flight sample. The 20-μm scan was taken near the bottom of the PT sample, near the top of the GBT sample, and near the hot end of the flight sample.

A large difference in microhardness between the primary compound phase and the secondary

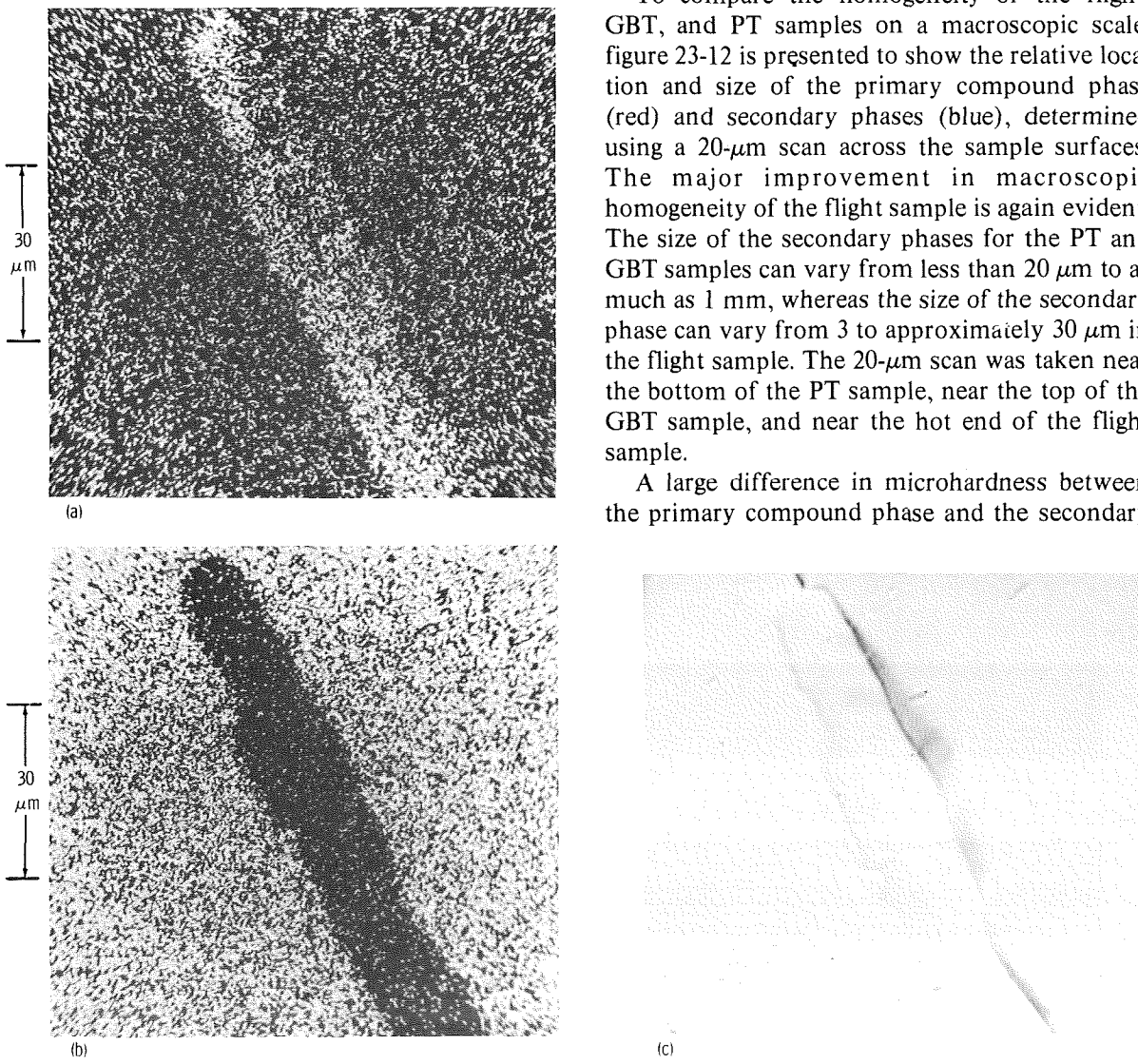

FIGURE 23-10.—SEM/EDAX map of flight AlSb sample (A-185). (a) EDAX Al scan. (b) EDAX Sb scan. (c) SEM photograph.

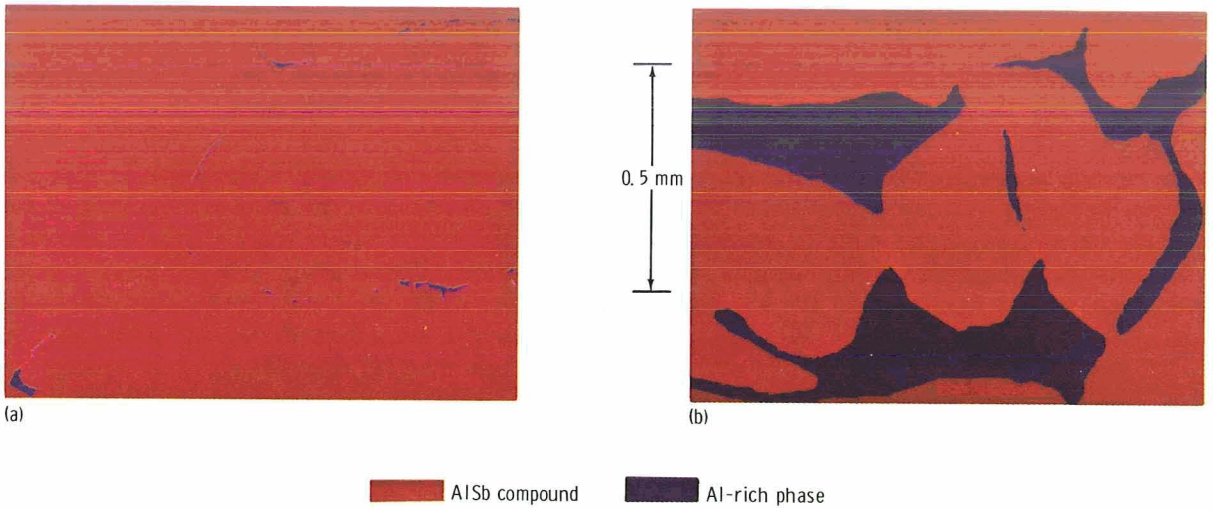

FIGURE 23-11.—Pseudocolor photographs showing microstructures of flight and GBT AlSb samples. (a) Low-g sample (A-185). (b) One-g sample (A-141).

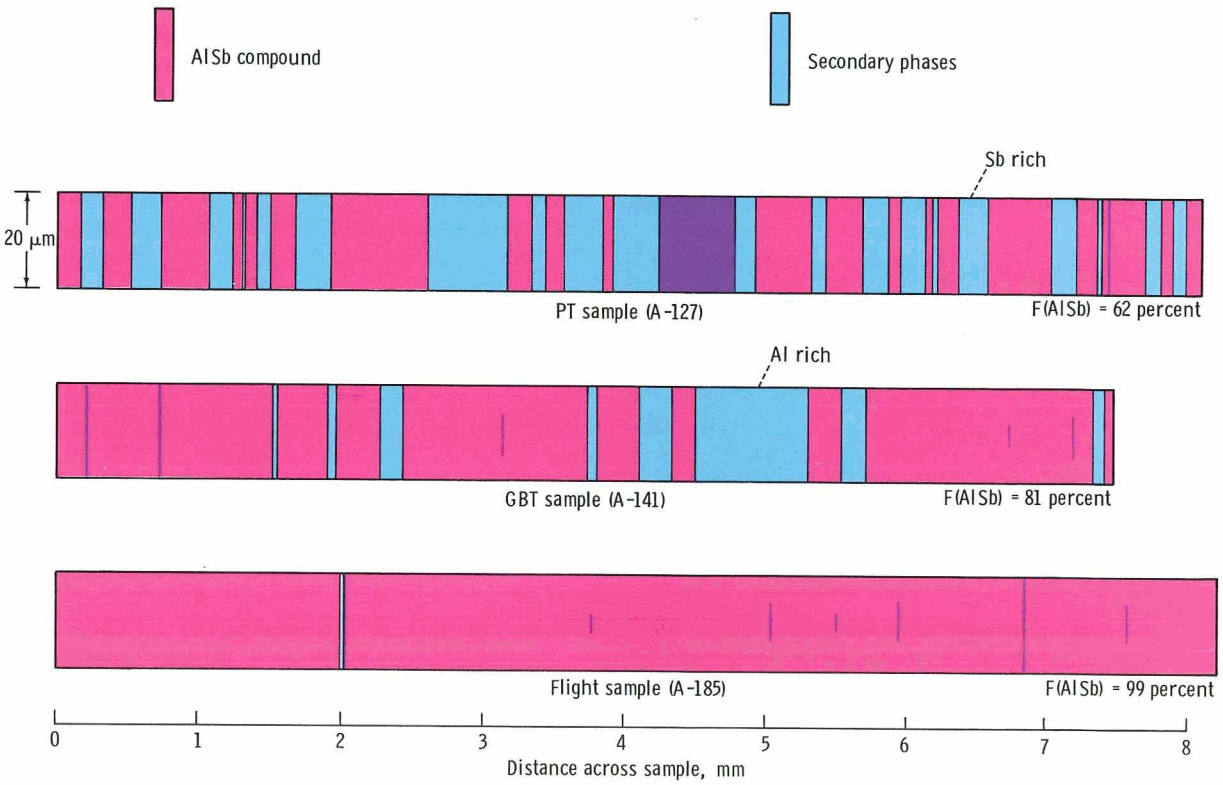

FIGURE 23-12.—Distribution of compound and secondary phases across low-g and one-g AlSb samples determined using 20-μm scan. The symbol F(AlSb) represents the primary compound concentration.

phase also is evident. Microhardness readings taken on a PT sample section indicate that the AlSb phase has a Vickers number of approximately 400, whereas the softer second phase has a hardness number of approximately 60.

Quantitative microstructural and chemical analysis.—To obtain a more quantitative comparison of the microstructure, a continuous series of photomicrographs (100×) was taken across the sectional surface of flight sample A-185 and GBT sample A-141. An area analysis for the secondary phase, obtained from the photomicrographs, is shown in figure 23-13. The area fraction of the secondary phase varies from approximately 2 to 22 percent for the GBT sample. As shown in figure 23-13, the secondary phase is nonuniformly distributed on a macroscopic scale for the GBT sample. For the flight sample, the area fraction varies from approximately 0.7 to 2 percent. Thus, the flight sample is macroscopically much more homogeneous than the GBT sample. Note, also, that the least homogeneous portion of the flight sample contains no more of the secondary phase than the most homogeneous portion of the GBT sample. As also shown in figure 23-13, the ratio of the average area fraction of the GBT sample to the average area fraction of the flight sample is 5.1. One photomicrograph each from the GBT and flight samples was selected to quantitatively compare the microscopic homogeneity of the material. For these selected regions of the samples, the area fraction of the AlSb compound phase was determined as a function of measured area. The results are shown in figure 23-14, which reveals that the flight sample is also more homogeneous in terms of the microscopic areas examined. The average size of the secondary phase was determined for the same photomicrographic data, and the results are shown in figure 23-15. On the average, the secondary phase is 33 times larger in the GBT sample than in the flight sample.

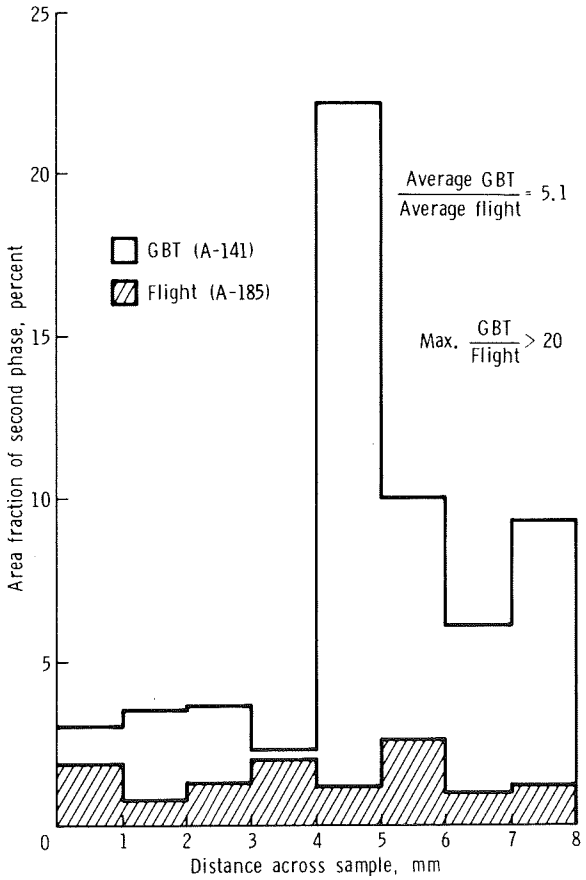

FIGURE 23-13.—Area fraction of secondary phases across flight and GBT AlSb samples.

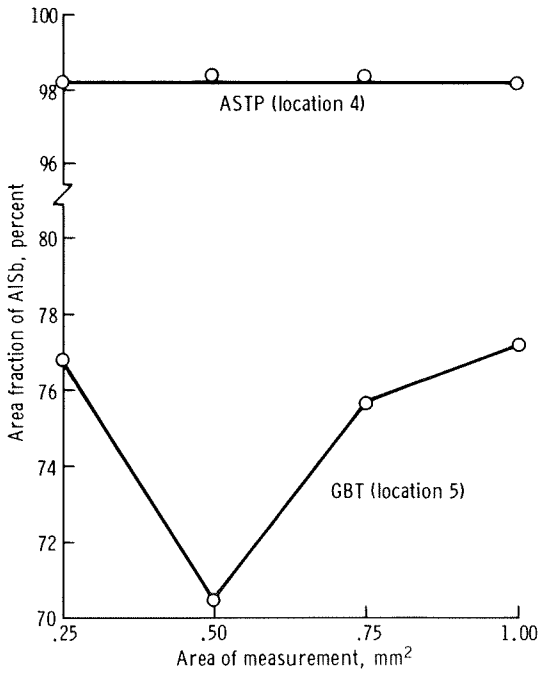

FIGURE 23-14.—Area fraction of compound phase as a function of measured area.

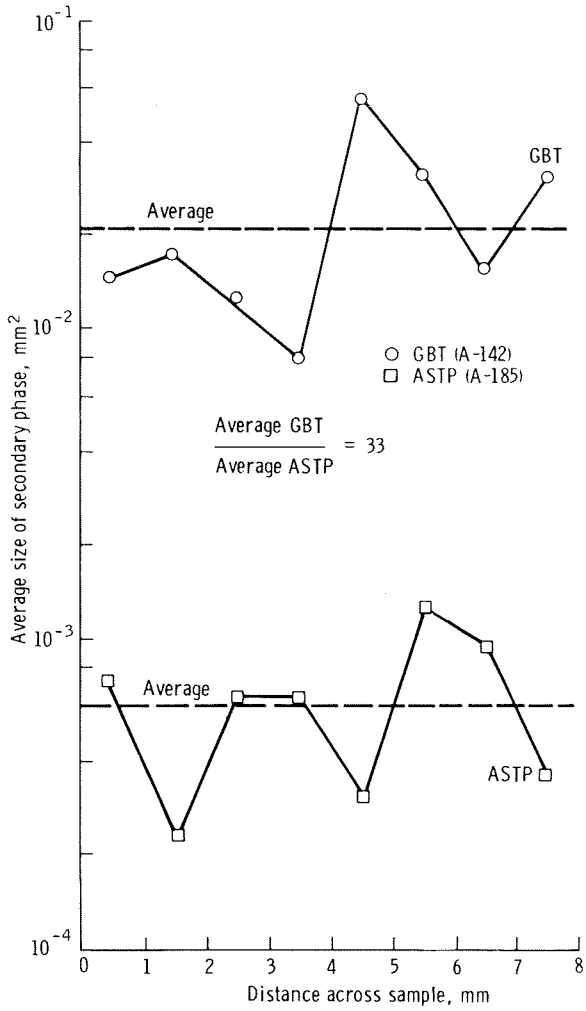

FIGURE 23-15.—Comparison of average size of secondary phases.

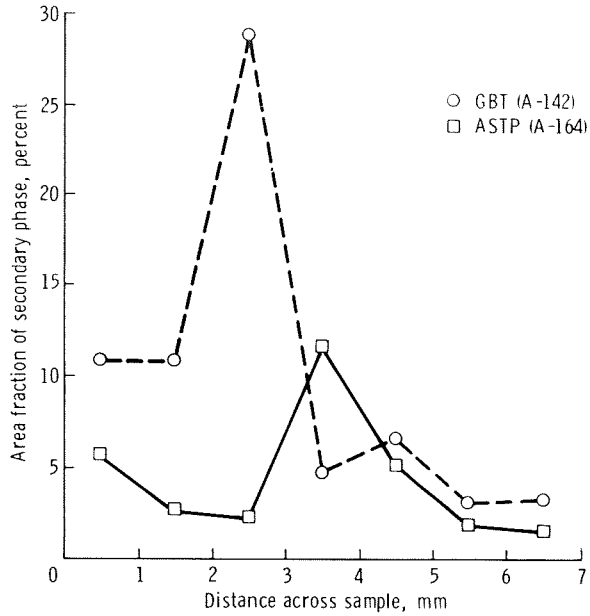

FIGURE 23-16.—Comparison of area fraction of secondary phases for the worst region of flight sample A-164 and a typical region of GBT sample A-142.

A similar quantitative microstructural analysis was performed on flight sample A-164 and GBT sample A-142. The least homogeneous portion of the flight sample was selected for this comparison, and the average reduction in the secondary phase is 2.2 times. The distributions of the second phase across representative segments of the two samples are plotted in figure 23-16.

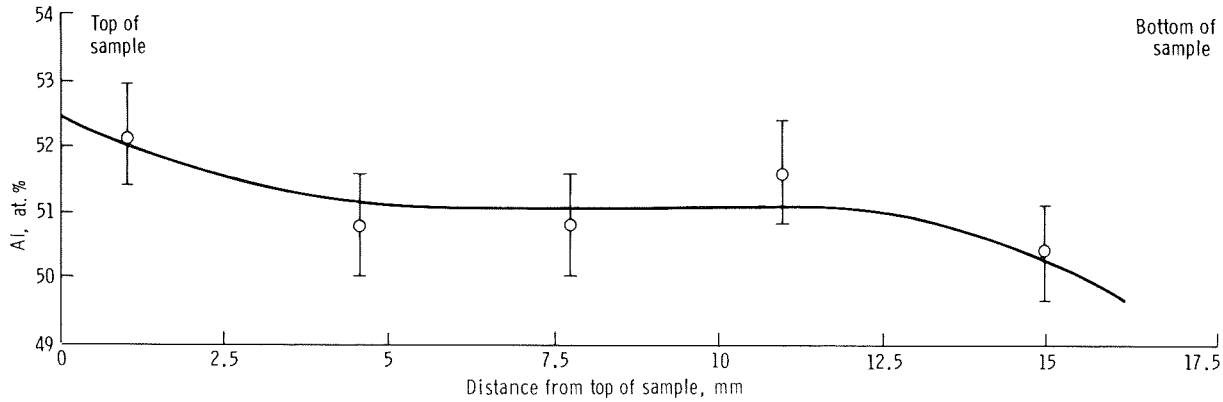

FIGURE 23-17.—Aluminum content in GBT AlSb sample (A-165) based on atomic absorption spectroscopy.

A third GBT sample (A-165) was cut into five wafers, which were analyzed for aluminum content using the method of atomic absorption spectroscopy. Results of this quantitative analysis are plotted in figure 23-17 as a function of distance from one end of the sample to the other end. It should be noted that the average Al content in this one-g-processed sample is approximately 1 at.% higher than the theoretical value and that there is a compositional variation from end to end, due perhaps to the influence of gravity during liquid-phase homogenization.

Because the initial SEM/EDAX results gave indications of variation in composition of the two microstructural phases in various samples, an effort has been initiated to use the ion-microprobe mass analyzer (IMMA) for quantitative chemical determination on a microscale. The preliminary IMMA results on PT sample A-132 are plotted in figure 23-18 in terms of ratios of Al^+ to Sb^+ ions sputtered off from the two phases at three locations. Because a "standard" has yet to be introduced, these results are considered as semi-quantitative in nature. Nevertheless, the differences in the Al/Sb ratios are significant, indicating that the second phase in this sample has varying compositions from one end of the sample to the other, and that the AlSb compound phase may have a small homogeneity range not unlike many other intermetallic compounds such as Cu_3As, AgZr, BeCo, AlLi, or $AlPd_2$.

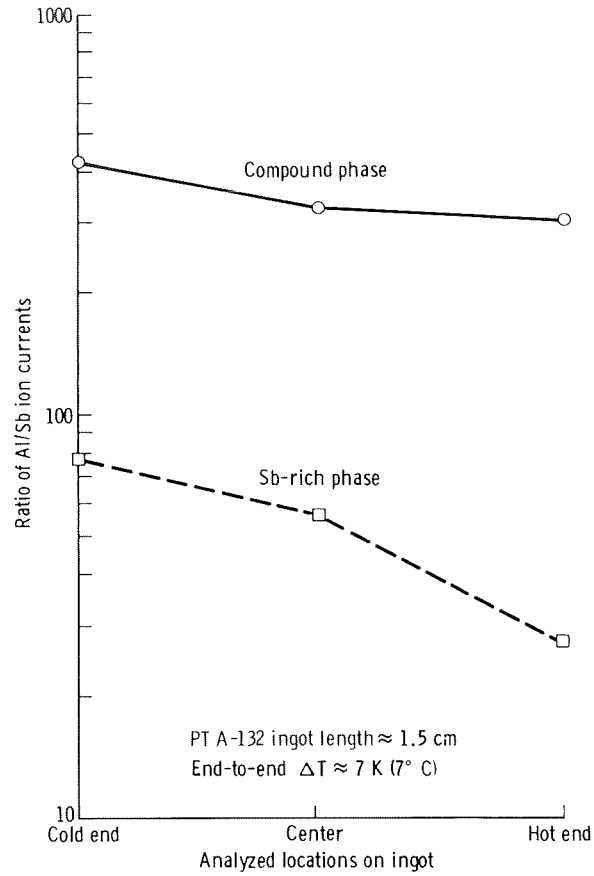

FIGURE 23-18.—IMMA Al/Sb ratios in PT AlSb sample.

Figure 23-19 contains IMMA ion maps for Sb^+ in the second phases for a low-g and a one-g sample. A comparison of the maps shows that, in the flight sample, the small amount of residual second phase is almost pure Al; whereas, in the GBT sample, the Al-rich phase does contain significant concentrations of Sb.

Electrical resistivity.—Aluminum antimonide is a Group III-V semiconducting compound with a typical resistivity (p type) of 10 to 100 Ω cm. The Al-rich and Sb-rich phases are metallic and should have resistivity values in the range of 10^{-4} to 10^{-6} Ω cm (i.e., the resistivity of the secondary phases would depend on their precise composition and previous history). Thus, the average resistivity of the AlSb samples would be very sensitive to the relative fraction of the primary compound phase and the secondary phases, because the compound phase has a resistivity that is six orders of magnitude larger than the resistivity of the secondary phases. Likewise, those samples that have the largest values of resistivity should contain the highest fraction of the compound phase.

By measuring the resistivity on a cut and polished surface of the sample using a four-point probe, the localized values of resistivity obtained will be a sensitive indication of the quality for the sample at various locations within the material. The electrical resistivity of two prototype samples and one flight sample was determined by using a four-point probe to measure approximately 10 to 20 values at different locations on each sample. The results are shown in table 23-II. The typical or average value of resistivity found for the flight sample was 12 Ω cm, which indicates that the flight sample consisted almost entirely of the

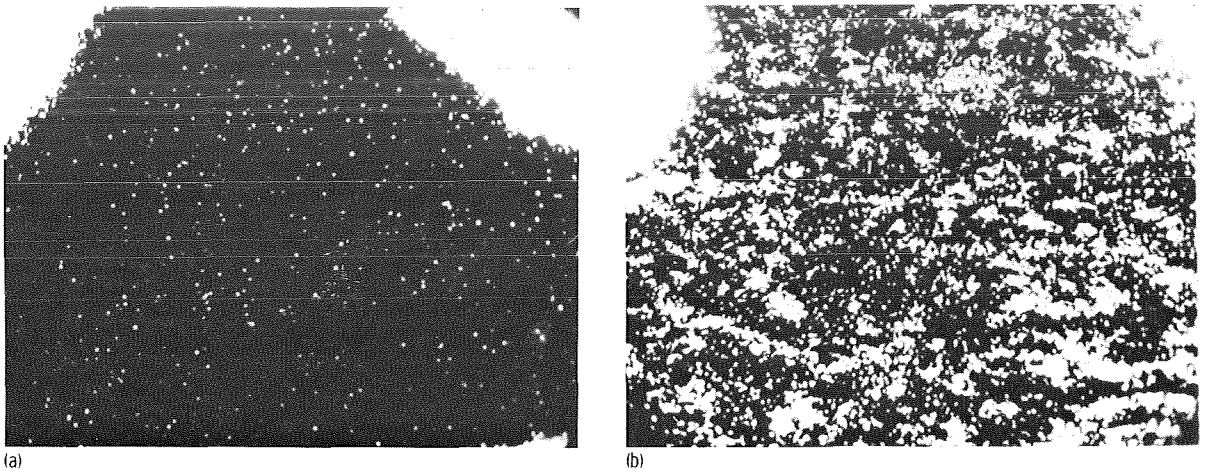

FIGURE 23-19.—IMMA Sb^+ ion maps for Al-rich phase of flight and GBT AlSb samples. The white areas in the upper corners are the AlSb compound phase. (a) Low-g sample (A-185), 1326×. (b) One-g sample (A-141), 975×.

TABLE 23-II.—Resistivity of AlSb Samples

Sample	*Resistivity, Ω cm*	
	Typical value	*Minimum value*
Flight (A-185)	12	0.03
PT (A-132)	.009	.003
PT (A-127)	.003	.002

compound phase. The minimum or "worst" value of resistivity of 0.03 Ω cm found in the flight sample is still a factor of 3 to 10 greater than typical values observed in the two PT samples. The PT samples had typical resistivity values in the range of 3×10^{-3} to 9×10^{-3} Ω cm, which is three orders of magnitude less than expected for the pure compound phase but also several orders of magnitude larger than expected for the secondary phases. Thus, the resistivity measurements tend to support the results and conclusions of the microstructural studies. That is, the flight sample shows major improvements in compositional homogeneity. Additional measurements will be made on the GBT samples.

X-ray diffraction studies.—A small amount of material was filed off the outside surface of one flight sample (A-164) at both the top and the bottom, one GBT sample (A-141) at the middle, one PT sample (A-124) at the bottom, and at two locations from a single crystal of AlSb. The single crystal, which actually consisted of several twins or large single crystalline grains, was obtained from the Battelle Memorial Institute (BMI) for the purpose of comparative characterization. This crystal is assumed to be unique, since the authors have not been able to find any other single crystals of AlSb. Using the Debye-Scherrer technique, X-ray diffraction images were made with Cu K_α radiation through a nickel (Ni) filter. An optimum exposure time of 2 hours was chosen after verification that a 4-hour exposure time did not reveal additional lines but, instead, increased the background fluorescence. The main results of this analysis are summarized in table 23-III.

All samples, except for PT sample A-124, revealed only the AlSb compound lines. The bottom part of PT sample A-124 had eight additional lines that could be identified as Sb lines. As expected, the lattice constant of AlSb for all samples was the same to within an accuracy of ±0.0003 nm and agreed with the best published data (ref. 23-14) and the data of the single crystal. A careful measurement of the highest reflection lines indicated that the primary phase was always forming at the 50 ± 1 at.% stoichiometric composition. That is, to within an accuracy of 1 at.%, the composition of the compound does not appear to vary between samples or to depend on the extent or the nature of the secondary phases.

TABLE 23-III.—*X-Ray Diffraction Study of AlSb Samples*

Sample (location)	*Lattice constant, nm*	*Notes*
Flight A-164 (top)	0.6133 ± 0.3	AlSb lines
(middle)	.6134 ± .3	AlSb lines
GBT A-141 (middle)	.6133 ± .3	AlSb lines
PT A-124 (bottom)	.6135 ± .3	AlSb lines + Sb lines
BMI single crystal (no. 1)	.6136 ± .3	AlSb lines
(no. 2)	.6136 ± .3	AlSb lines
Published data (ref. 23-14)	.61355 ± .01	

Liquid-state homogenization and diffusional analysis.—The observation that the ASTP samples have a much smaller amount of the secondary or satellite phases compared to ground samples seems to suggest the following: at low-g, intermetallic diffusion dominates in the liquid-state homogenization process; whereas, at one-g, convection-induced segregation hampers the process of compositional homogenization. The results obtained can be explained by assuming that the low-g melts are relatively well homogenized within the 1.5 hours of available diffusion time but that the one-g melts are still relatively inhomogeneous after 1.5 hours. The inhomogeneities that seem to exist in the Earth-based melts are probably caused by the large differences in densities that exist between the Al-rich and Sb-rich phases found in the best commercially available starting material (fig. 23-4).

Based on the preceding premises, a liquid-state homogenization model for the AlSb system may be postulated to analyze the relative importance of gravity and diffusion. Because the starting material consists of Al-rich, Sb-rich, and AlSb phases, some time will be required for liquid-state diffusion to homogenize the material at every location within the melt. If during this time, the Al- and Sb-rich liquid phases are separating or segregating as a result of gravity-driven convection caused by differences in density, the compositional inhomogeneities within the melt may increase. To determine whether gravity or diffusion is the dominant process, a liquid-state homogenization number H may be defined as a convective or segregation distance divided by diffusion distance. If $H >> 1$, gravity will dominate; if $H \approx 1$, gravity will have a smaller effect; and if $H << 1$, diffusion will dominate. Consider a region of the melt having typical size ℓ and having a density difference $\Delta\rho$ from the surrounding AlSb melt defined as

$$\Delta\rho = \rho_{AlSb} - \left[C\rho_{Al} + (1 - C)\rho_{Sb}\right] \qquad (23\text{-}1)$$

where C is the concentration of Al in the inhomogeneous region. If a Stokes' law type of model is used to specify the convective distance and a Fick's law type of model to specify the diffusional distance, then

$$H = \frac{\ell^2 \Delta\rho g}{5\nu} \sqrt{\frac{t_s}{D}} \qquad (23\text{-}2)$$

where ν is the viscosity of the primary fluid phase, g is acceleration due to gravity, and t_s is the total soak time for a melt at diffusion rate D. To determine the influence of gravity relative to diffusion, consider a conservative analysis (which would tend to underestimate the gravitational influences) by selecting $\ell \leq 0.2$ mm, $C \approx 0.9$, $D \approx 10^{-4}$ cm^2/sec, $\nu \leq 1$ N sec/m^2 (10 P), and $\Delta\rho \approx 2$ g/cm^3. Based on these values, $H \gtrsim 100$ for the ground-based test and $H \lesssim 0.1$ for the flight test (assuming 10^{-3}g).

Thus, these calculations would tend to indicate that convection has an important role in maintaining any inhomogeneities that may exist in Earth-based AlSb melts. Conversely, if the inhomogeneities are localized and if the starting

material is on the average macroscopically 50 at.% of each element, then the calculations would tend to indicate that the melt should rapidly homogenize by liquid-state diffusion in a low-g environment.

These simple calculations are useful in identifying the difficulties of maintaining homogeneous Earth-based melts. It should also be understood that part of the effects observed in this experiment may occur during the nucleation, growth, and solidification of the compound phase.

Lead-Zinc Immiscible System

Results of the Pb-Zn experiments are discussed in the following paragraphs.

Miscibility gap in the Pb-Zn system.—The Pb-Zn system is a classical monotectic binary characterized by a large liquid miscibility gap in the temperature-composition phase diagram. (See fig. 23-1.) Thermodynamically, the two liquids within the immiscible region do not obey the normal solution laws and exhibit large positive deviations from Raoult's linear relationship between activity and concentration. In this miscibility gap, on an atomic scale, the dipole-dipole attractive forces between like atoms (or ions) are much greater than between unlike species. With the large difference in specific gravity (Pb/Zn = 11.34/7.14), macroscopic sedimentation of the heavier Pb liquid occurs when the binary melt is held quiescently on Earth in the miscibility gap.

As described previously, the composition selected for the experiment is 20 at.% Pb or 33.2 percent Pb by volume. For this composition, the consolute temperature (immiscible to miscible transition point) is approximately 1068 K (795° C). The starting sample configuration was a layered ingot achieved by heating Pb on top of Zn in the graphite crucible at a temperature of 1123 K (850° C) for 10 minutes, resulting in the sedimentation of Pb through the Zn. Reheating samples of this type under low-g conditions for 60 minutes at a temperature 50 K (50° C) higher than the consolute temperature should promote miscible liquid interdiffusion. It was postulated that, by solidifying the thoroughly interdiffused liquids under low-g conditions, a microstructure consisting of a dispersion of superconducting Pb in the Zn matrix would be obtained.

The discussions to follow will reveal two important phenomenological observations that must be considered in future investigations (on Earth as well as in space) of immiscible systems similar to Pb-Zn. The first observation is that microscopically complete and total separation of Pb and Zn is difficult to achieve under one-g conditions. The second observation is that, under low-g conditions whereby convection is minimized, the liquid diffusion coefficient within the miscibility gap is smaller than commonly found for miscible metals.

Because of small convection currents, the precise measurement of liquid diffusion parameters in Earth experiments is extremely difficult. However, it is generally agreed that diffusion rates of liquids are orders of magnitude greater than those for the solid phases of the same components. It is also recognized that although the intermolecular geometry of diffusing liquids is not well understood, some geometric order does exist in liquids having similar properties. If one assumes that a range of liquid diffusion lengths exists, an analysis of the root mean square (rms) distance covered by atoms as a function of time will lead to an expression similar to that for the long-range atomic motion in one-dimensional solid diffusion. This liquid diffusion motion in terms of rms distance covered is

$$\overline{x^2} = 2Dt \qquad (23\text{-}3)$$

where D is the liquid diffusion coefficient and t is time. The available experimental data reported in the literature show that liquid metal diffusion coefficients all fall within the range of 10^{-5} to 10^{-4} cm^2/sec. It was on the basis of this knowledge that optimum mixing of Pb and Zn at a temperature of 1123 K (850° C) was postulated for the soaking period of 1 hour in the ASTP experiment.

The difference between diffusion profiles in miscible liquids (i.e., temperature T greater than consolute temperature T_C) and immiscible liquids

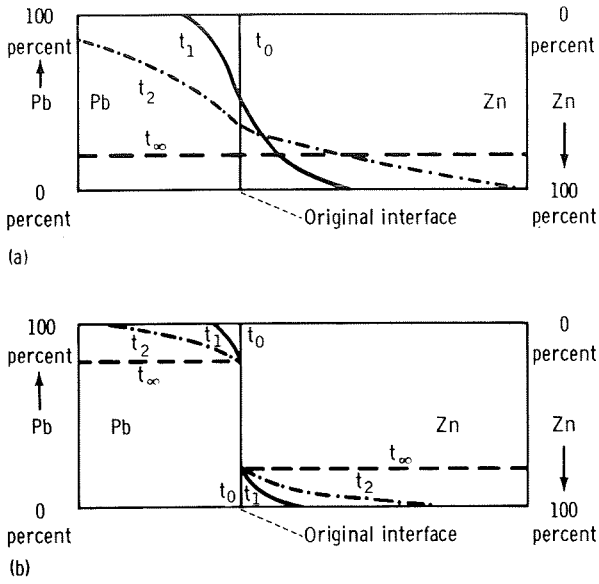

FIGURE 23-20.—Low-g Pb-Zn liquid-state diffusion models. (a) Miscible liquids ($T > T_C$). (b) Immiscible liquids ($T < T_C$).

($T < T_C$) is shown in figure 23-20. The models in figures 23-20(a) and 23-20(b) represent the expected diffusion profiles at times $t_\infty > t_2 > t_1$ for liquids diffusing from a well-defined interface starting at time t_0. For miscible liquids, the original interface should quickly disappear or become modified and the concentration gradient should vary continuously and smoothly throughout the sample. After a sufficient time lapse (i.e., identified as t_∞), the two liquids should homogenize into one liquid phase. In contrast to miscible liquids, the model in figure 23-20(b) indicates that the original interface should persist for immiscible liquids even for long diffusion times (t_∞), and that there should be a discontinuity in the concentration gradient at the interface. Within the miscibility gap, the diffusion profiles on both sides of the interface would probably approach those for solid-state diffusion as described by the second Fick's law for change in solute concentration C as a function of time and distance

$$\frac{\partial C}{\partial t} = D \frac{\partial^2 C}{\partial x^2} \qquad (23\text{-}4)$$

where D is again the diffusion coefficient. By analyzing the concentration of Pb in Zn, away from the interface, it should be possible to determine whether the analytical data agree with a solution of equation (23-4) in the form of

$$C = C_0 \left[1 - \operatorname{erf}\left(\frac{x}{2\sqrt{Dt}}\right)\right] \qquad (23\text{-}5)$$

where C_0 is the maximum solubility of Pb in Zn and x is the distance from the interface. In the discussion of the results that follow, it will be seen that the Pb-Zn system is still immiscible in a near-zero-g environment at a temperature 40 K (40° C) higher than the published value of the consolute temperature and that the diffusion coefficient is one or two orders of magnitude smaller than usually found in Earth-based liquid metals experiments.

Metallography and microanalysis.—The GBT samples show almost total and complete separation of the Pb and Zn phases, as can be seen in figure 23-21(a) for a polished and etched (using 5 percent nitric acid (HNO_3)) sample. Notice that the ASTP samples also show major separation of the Pb-rich and Zn-rich phases, as shown in figure 23-21(b). Consistent with the immiscible-liquids model of figure 23-20(b), the original Pb/Zn interface is evident. An SEM photograph of the interface on the flight sample is shown in figure 23-22(c); corresponding EDAX microchemical maps of Zn and Pb are also shown in figures 23-22(a) and 23-22(b), respectively. There appears to be a sharp discontinuity in the Pb and Zn concentrations at the interface. The black particles in the upper part of figure 23-22(c) are Pb particles dispersed in a Zn matrix.

The microstructure of the Zn-rich region is shown in figure 23-23 for polished and etched surfaces of the flight sample. Many of the particles seen in the photomicrograph are Pb-rich, as shown by the SEM photographs and EDAX maps of figure 23-24 (flight sample) and figure 23-25 (PT sample). The Pb dispersions in Zn appear to have a higher particle number density in the flight samples. The Pb particles of the flight sample also appear to be more uniform in size and spherical in shape. The particle alinement, evident in figure

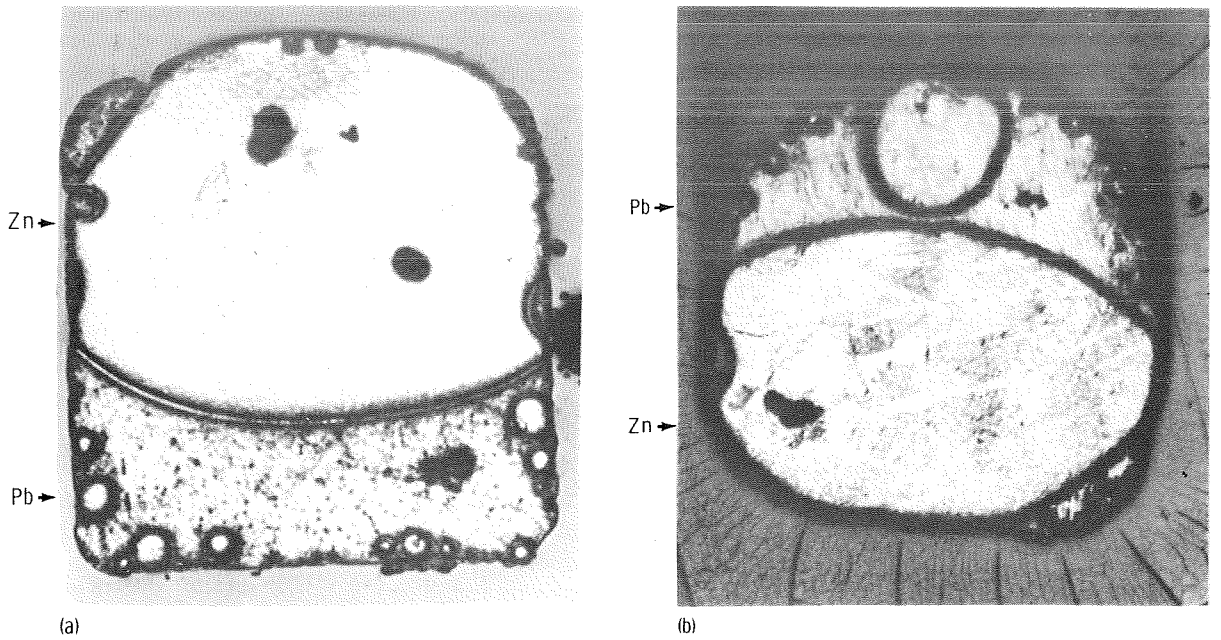

FIGURE 23-21.—Photomacrographs of Pb-Zn flight and GBT ingots. The Pb-rich and Zn-rich portions of the GBT ingots are reversed because of sedimentation. (a) One-g sample (gravity vector downward). (b) Low-g sample.

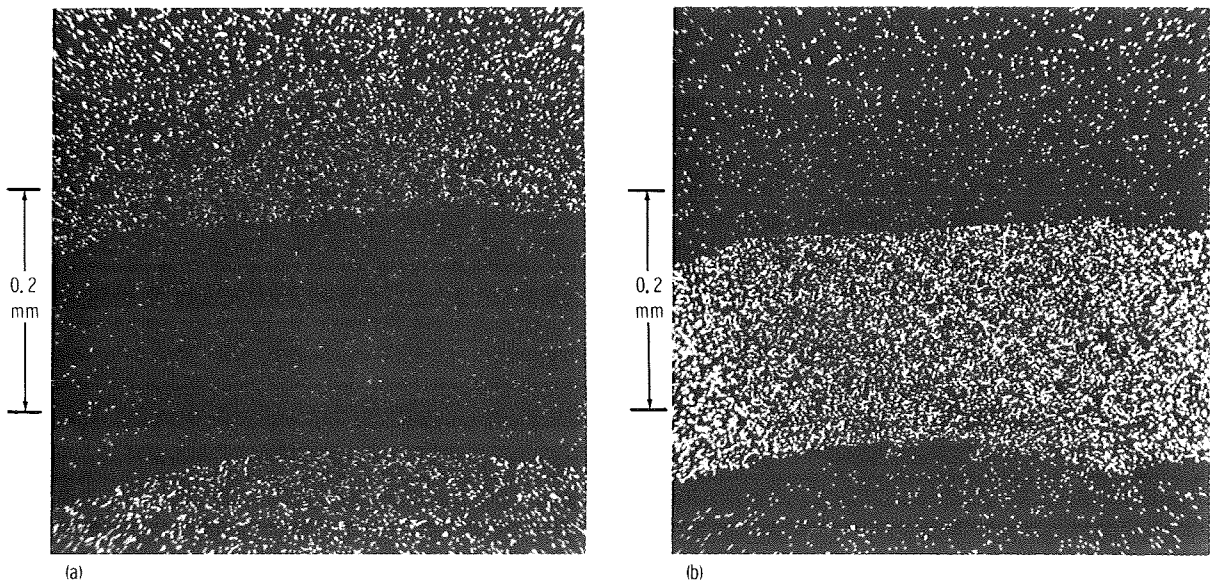

FIGURE 23-22.—SEM/EDAX maps of Pb/Zn interface in flight sample B-186. (a) EDAX Zn scan (L_{α}). (b) EDAX Pb scan (M). (c) SEM photograph.

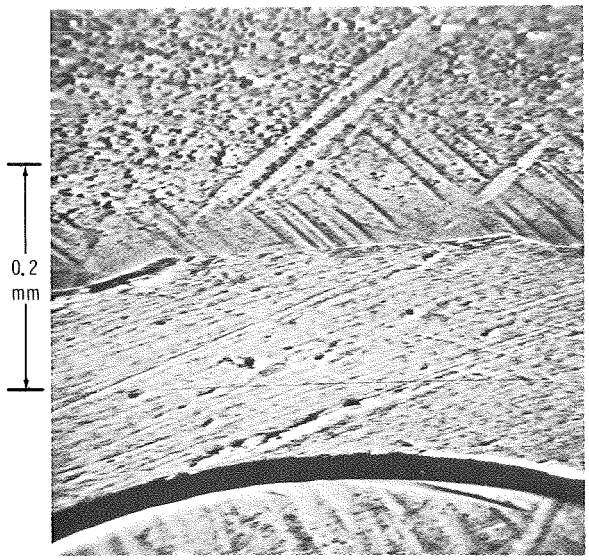

(c)

FIGURE 23-22.—Concluded.

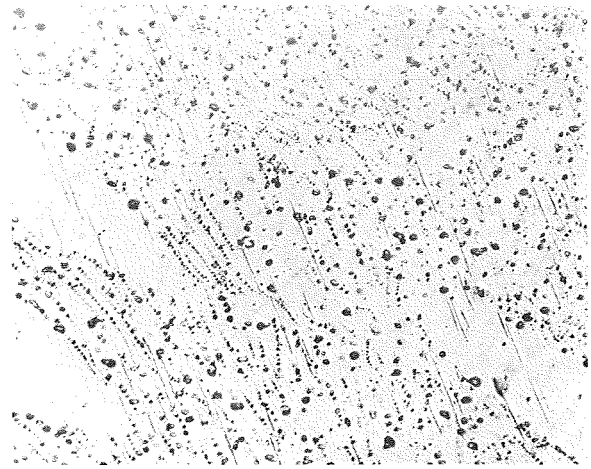

FIGURE 23-23.—Microstructure of flight Pb-Zn sample (32×).

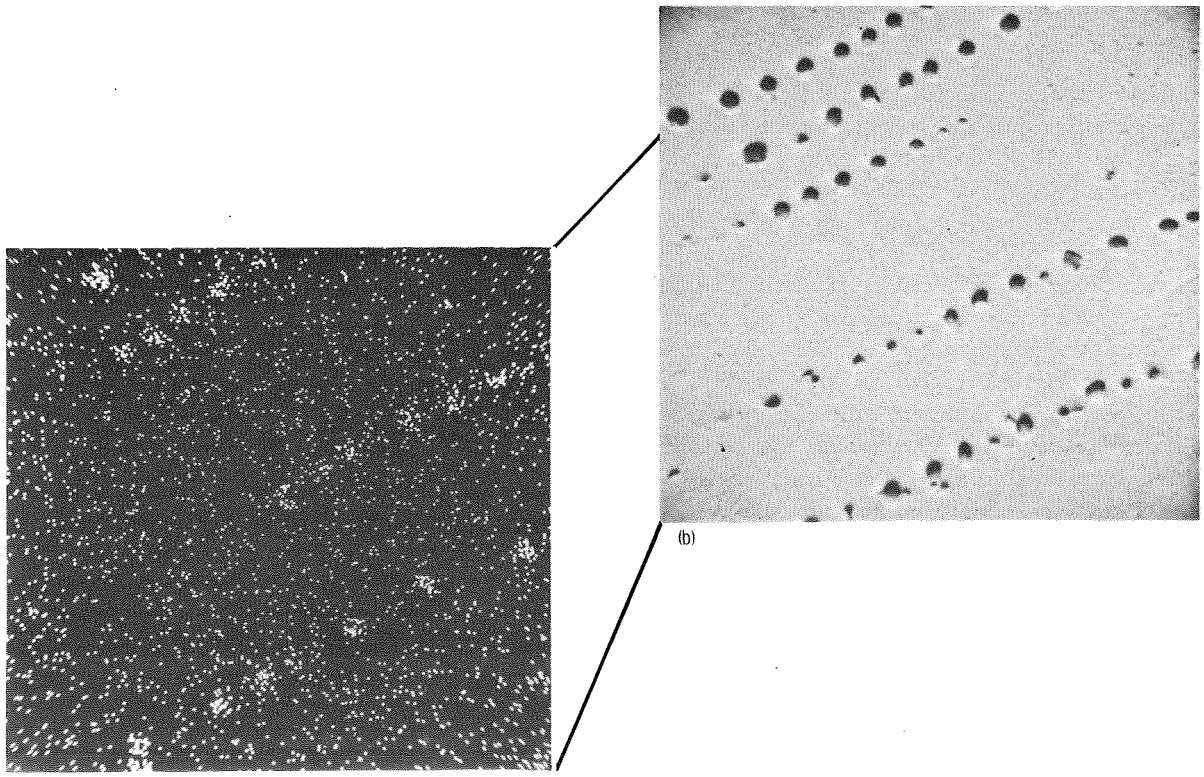

(a)

(b)

FIGURE 23-24.—SEM/EDAX map of Zn matrix in flight sample B-186. (a) EDAX Pb scan (M_α, M_β) (760×). (b) SEM photograph (654×).

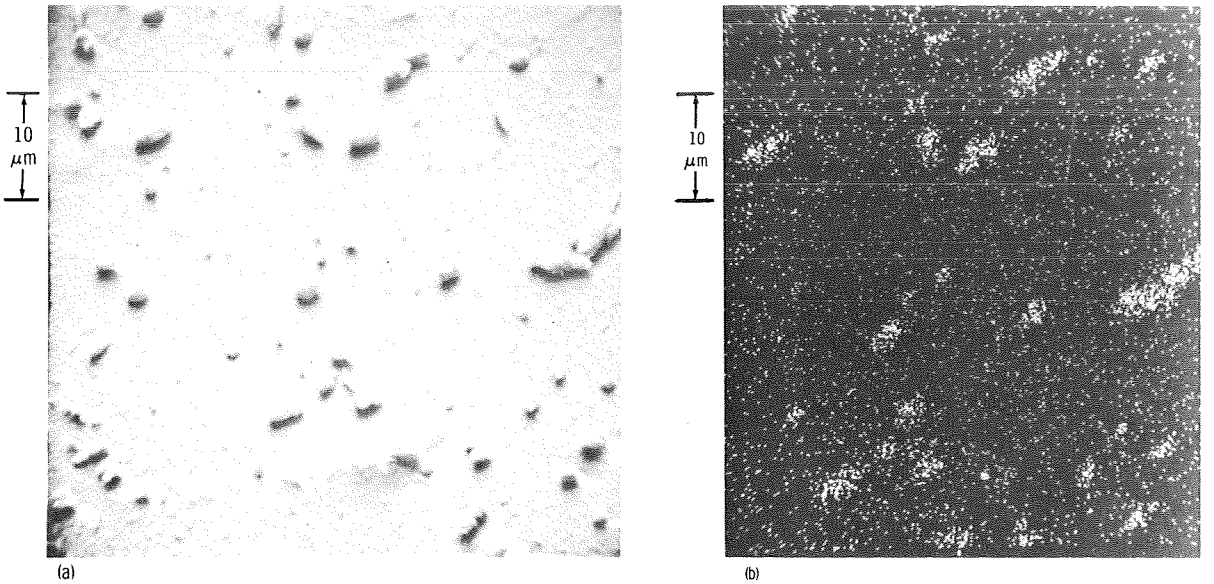

FIGURE 23-25.—SEM/EDAX map of Zn matrix in PT sample B-125. (a) SEM photograph (1332×). (b) EDAX Pb scan (M_α).

23-24(b), occurs in many of the flight samples and less in the GBT samples. It seems reasonable to attribute the alinement of the microstructure in the flight sample to constitutional supercooling and subsequent nucleation and growth of Pb particles along supersaturated fronts. As previously observed, this phenomenon would be expected to be less evident in the GBT samples because buoyancy forces acting on the individual particle and convective effects acting on the front would tend to destroy the alinement.

It should be noted that the one-g samples were processed in a manner to encourage convective mixing between the Pb and Zn phases. In the one-g samples, the more dense liquid Pb was initially on top of the less dense Zn, resulting in a flow of liquid Pb through the molten Zn. The residual Pb dispersions observed in the GBT samples indicate that total microscopic separation of the phases did not occur in one g. In the next section, it will be shown that the Zn-rich portion of a GBT sample has a dilute and approximately constant concentration of Pb, part of which could be in the monotectic phase.

Chemical and diffusional analysis.—One flight sample (B-186) and one GBT sample (B-165) were cut into small sections of approximately 3 mm^3 each (i.e., approximately 20 mg/section) such that the distance of each section away from the Pb-Zn interface could be determined. These small sample sections were chemically analyzed by means of atomic absorption spectroscopy. The results are shown in figure 23-26. The Zn matrix of the GBT sample (fig. 23-26(a)) contains only a small ($\approx$0.5 at.%) and constant concentration of Pb throughout the Zn matrix. This small concentration of Pb represents the combined influence of convective phase mixing during the heatup and soak period and density sedimentation of molten Pb particles during cooldown portions of the experiment. In contrast, the flight sample (fig. 23-26(b)) contains a relatively large (maximum concentration, 3.5 at.%) and monotonically decreasing concentration of Pb away from the Pb/Zn interface.

The data on the flight sample are consistent with the low-g immiscible-liquids diffusion model described in the subsection entitled "Miscibility gap in the Pb-Zn system" and specified by equation (23-5). Equation (23-5) can be best fitted to the data by assuming an equilibrium concentration at the interface C_0 of 8 at.% and a diffusion coefficient of 2.4×10^{-6} cm^2/sec. The theoretical immiscible-liquids diffusion curve is shown in

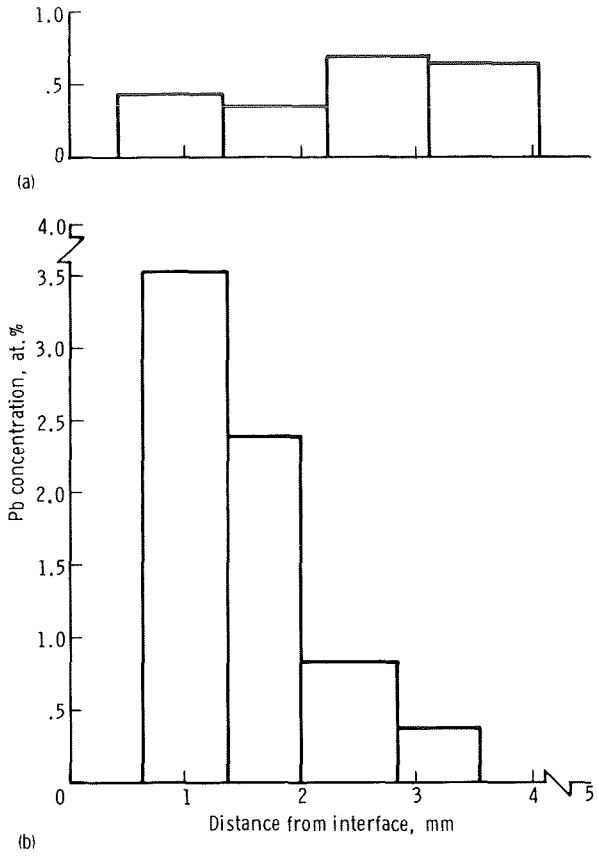

FIGURE 23-26.—Compositional profiling of GBT and flight Pb-Zn samples based on atomic absorption spectroscopy. (a) GBT-2 sample (B-165). (b) ASTP sample (B-186).

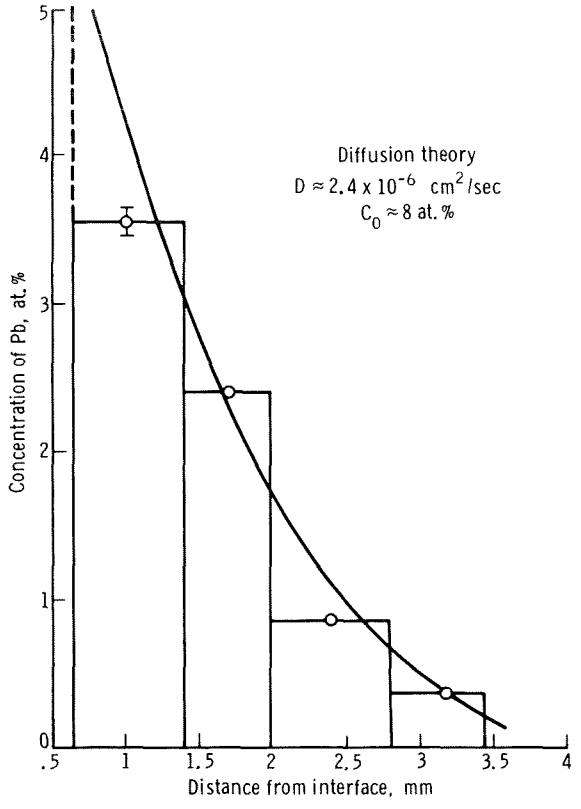

FIGURE 23-27.—Diffusion profile for concentration of Pb in Zn matrix in flight sample. The curve is an optimum fit to the data, based on an immiscible-liquids diffusion model.

figure 23-27. After several attempts, it was concluded that the data could not be fitted with a miscible-liquids diffusion model. The results of the chemical and diffusional analysis is therefore consistent with the microchemical and metallographic analysis in that the combined results show, in the low-g experiment, that Pb and Zn are still immiscible at a temperature of 1108 K (835° C) and that the diffusion coefficient measured in the low-g sample is one or two orders of magnitude smaller than commonly expected. Thus, these experimental results would suggest that there is a significant inaccuracy in the published phase diagram of Pb-Zn.

Pelzel (ref. 23-15) has measured the rate of solution K in both immiscible and miscible liquid metals. His results appear to follow the diffusion models given in the subsection entitled "Miscibility gap in the Pb-Zn system," and he finds that values of K for the monotectic systems are the same order of magnitude as in experiments in which one of the phases is a solid reaction partner. He also finds that K is influenced by buoyance or gravitational effects. Using Pelzel's published value of K for the diffusion of Pb and Zn at a temperature of 773 K (500° C), it is estimated that his Earth-based experiment had an effective diffusion coefficient, $D \approx 3 \times 10^{-4}$ cm^2/sec, which is two orders of magnitude greater than observed in the ASTP experiment. Thus, the combined results of the low-g experiment and Pelzel's one-g experiment would tend to support the conclusion that liquid metal diffusion is strongly influenced by thermal or density-driven

convection in Earth-based experiments and that, in the low-g experiment, the probability is high that the homogenization temperature of 1108 K (835° C) was not above the miscibility gap.

In summary, the results of the chemical and diffusional analysis would tend to indicate that the Pb-Zn part of the experiment did not perform as initially anticipated for two reasons. First, the Pb-Zn system is apparently still immiscible at a temperature of 1108 K (835° C), which would limit the concentration gradient in the samples and greatly reduce the rate of solution K. Second, the diffusion coefficient D is much smaller than was initially expected. The results of the experiment do suggest that the low-g quiescent environment of space is an ideal environment for accurately determining diffusional and kinetic reaction rates that may be difficult, or perhaps in some cases impossible, to determine on the ground.

Electrical resistivity.—The previous results and conclusions must be modified if the Pb-Zn samples contained oxides at the interface; such a condition would tend to prevent interdiffusion. The existence of oxides seems improbable because only the highest purity materials were used, the ampoules were sealed under high-purity argon, and previous PT and GBT experiments did not indicate the presence of oxides. Moreover, the sedimentation of Pb through Zn during the initial stage of sample preparation would break up oxide films if present in the starting materials. However, to further test for the presence of oxides at the Pb/Zn interface, a sensitive test that involved measuring the average resistivity of the material in the vicinity of the interface was performed.

The resistivity of the materials was measured on the mounted, polished, and etched sample surfaces using a four-point probe. One flight sample (B-186) and one GBT sample (B-142) were selected for the test. The results of the measurements are presented in figure 23-28, where each measurement point represents the average of 10 separate determinations. The absolute accuracy of the measurement is approximately 5 percent, and the relative accuracy between points is better than 1 percent. Both the ASTP and the GBT resistivity values varied smoothly and continuously across the interface. In neither case was there any evidence of any oxide layer along the interface. The slightly larger resistivity values associated with the flight sample near the interface were probably caused by the higher concentration of Pb in the Zn matrix found by the chemical analysis.

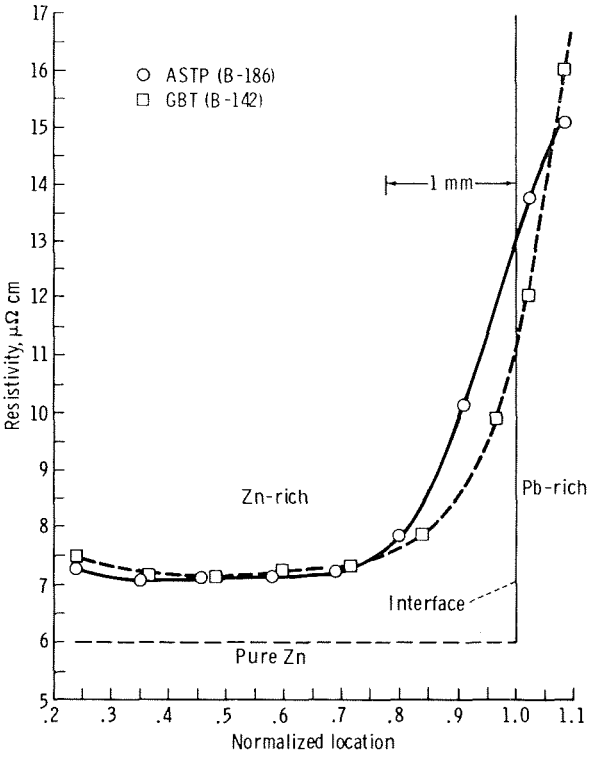

FIGURE 23-28.—Electrical resistivity of Pb-Zn samples.

CONCLUSIONS

The experiment plan for the ASTP Monotectic and Syntectic Alloys Experiment has been implemented, and the following conclusions have been reached.

Aluminum Antimonide Compound

1. Liquid-state homogenization of polycrystalline, multiphase AlSb in a low-g environment produces major improvements in macroscopic and microscopic homogeneity. The ASTP-processed material contains an average of 4

and a maximum of 20 times less of the unwanted secondary phase. Very small amounts of an Al-rich phase are found only along parts of the grain boundaries in the flight samples, whereas the ground-processed counterparts show major grains of the Al-rich or Sb-rich phase not unlike the starting material except for the recrystallized grain structure.

2. A diffusional and liquid-state homogenization analysis indicates that gravity-induced convection can severely complicate the homogenization of AlSb melts on Earth and can induce compositional and microstructural inhomogeneity during solidification.

3. Qualitative and semiquantitative energy dispersive X-ray and ion-microprobe mass analyses indicate the possibility of a homogeneity range for the AlSb compound and compositional variations in the secondary phases. A chemical analysis of a one-g sample indicates an overall approximate stoichiometric composition with a small, possibly gravity-induced, longitudinal variation in Al content.

Lead-Zinc Immiscible System

1. Incomplete liquid-state mixing of Pb and Zn was observed in the ASTP experiment, although the homogenization temperature of 1108 K (835° C) is 40 K (40° C) above the miscibility gap described in the literature. In the flight samples, a dispersion of fine particles of superconducting Pb in the Zn matrix was observed, but the bulk of Pb remained in the same position as before the start of the experiment. The experiment results suggest that there is a significant inaccuracy in the published phase diagram for Pb-Zn.

2. Compositional profiling of a low-g-processed sample indicates a quasi-solid-state diffusion of Pb into Zn with a diffusion coefficient of 2.4×10^{-6} cm^2/sec, which is about two orders of magnitude smaller than expected from ground-based experiments.

3. Difficulty in controlling convective mixing, sedimentation, and density gradients can hinder the analysis of diffusional or other kinetic processes in material systems performed on Earth. The quiescent low-g conditions of orbital flight provide an ideal environment for studying and accurately measuring such processes by reducing or eliminating the competitive gravity-dependent variables.

REFERENCES

23-1. Proceedings of the Third Space Processing Symposium on Skylab Results, vol. 1. NASA TM X-70252, 1974.

23-2. Proceedings of the Third Space Processing Symposium on Skylab Results, vol. 2. NASA TM X-70253, 1974.

23-3. Hansen, Max: Constitution of Binary Alloys. McGraw-Hill (New York), 1959, p. 1118.

23-4 Yates, I. C., Jr.: Apollo 14 Composite Casting Demonstration. NASA TM X-64641, 1971.

23-5. Lacy, L. L.; and Otto, G. H.: The Stability of Liquid Dispersions in Low Gravity. Paper No. 74-1242, AIAA/AGU Conference on Scientific Experiments of Skylab (Huntsville, Ala.), Oct. 30-Nov. 1, 1974.

23-6. Lacy, Lewis L.; and Otto, Guenther H.: Electrical Resistivity of Gallium-Bismuth Solidified in Free Fall. AIAA J., vol. 13, no. 2, Feb. 1975, pp. 219-220.

23-7. Reger, J. L.: Experimental Development of Processes to Produce Homogenized Alloys of Immiscible Metals, Phase III. NASA CR-149977, 1976.

23-8. Otto, Guenther: Studies on Immiscible Alloys. NASA CR-144226, 1976.

23-9. Willardson, R. K.; and Beer, Albert C., eds.: Semiconductors and Semimetals. Physics of III-V Compounds. Vol. 4. Academic Press (New York) 1968, p. 59.

23-10. Rittner, E. S.: Use of p-n Junctions for Solar Energy Conversion. Phys. Rev., vol. 96, no. 6, Dec. 15, 1954, pp. 1708-1709.

23-11. Loferski, J. J.: Theoretical Considerations Governing the Choice of the Optimum Semiconductor for Photovoltaic Solar Energy Conversion. J. Appl. Phys., vol. 27, no. 7, July 1956, pp. 777-784.

23-12. Ang, Choh-Y.; and Lacy, Lewis L.: Monotectic and Syntectic Alloys: ASTP Experiment MA-044. NASA TM X-64956, 1975.

23-13. Ang, C. Y.; and Lacy, L. L.: Monotectic and Syntectic Alloys: Experiment MA-044. Sec. 24 of the Apollo-Soyuz Test Project Preliminary Science Report. NASA TM X-58173, 1976.

23-14. Giesecke, Von G.; and Pfister, H.: Präzisionsbestimmung der Gitterkonstanten von $A^{III}B^{V}$-Verbindungen. Acta Cryst., vol. 11, 1958, pp. 369-371.

23-15. Pelzel, E.: Die Loesungsgeschwindigkeit Fester und Fluessiger Metalle in Ruhenden Schmelzen. Z. Metallk., vol. 61, no. 4, Apr. 1970, pp. 289-297.